Int J Earth Sci (Geol Rundsch) (2017) 106:1311–1340
DOI 10.1007/s00531-016-1311-6

ORIGINAL PAPER

The early Cretaceous orogen-scale Dabieshan metamorphic core complex: implications for extensional collapse of the Triassic HP–UHP orogenic belt in east-central China

Wenbin Ji[1,2] · Wei Lin[1] · Michel Faure[2] · Yonghong Shi[3] · Qingchen Wang[1]

Received: 1 October 2015 / Accepted: 19 February 2016 / Published online: 16 March 2016

Abstract The Dabieshan massif is famous as a portion of the world's largest HP–UHP metamorphic belt in east-central China that was built by the Triassic North–South China collision. The central domain of the Dabieshan massif is occupied by a huge migmatite-cored dome [i.e., the central Dabieshan dome (CDD)]. Origin of this domal structure remains controversial. Synthesizing previous and our new structural and geochronological data, we define the Cretaceous Dabieshan as an orogen-scale metamorphic core complex (MCC) with a multistage history. Onset of lithospheric extension in the Dabieshan area occurred as early as the commencement of crustal anatexis at the earliest Cretaceous (ca. 145 Ma), which was followed by primary (early-stage) detachment during 142–130 Ma. The central Dabieshan complex in the footwall and surrounding detachment faults recorded a consistently top-to-the-NW shearing. It is thus inferred that the primary detachment was initiated from a flat-lying detachment zone at the middle crust level. Removal of the orogenic root by delamination at ca. 130 Ma came into the extensional climax, and subsequently isostatic rebound resulted in rapid doming. Along with exhumation of the footwall, the mid-crustal detachment zone had been warped as shear zones around the CDD. After 120 Ma, the detachment system probably experienced a migration accommodated to the crustal adjustment, which led to secondary (late-stage) detachment with localized ductile shearing at ca. 110 Ma. The migmatite–gneiss with HP/UHP relicts in the CDD (i.e., the central Dabieshan complex) was product of the Cretaceous crustal anatexis that consumed the deep-seated part of the HP–UHP slices and the underlying para-autochthonous basement. Compared with the contemporaneous MCCs widely developed along the eastern margin of the Eurasian continent, we proposed that occurrence of the Dabieshan MCC shares the same tectonic setting as the "destruction of the North China craton". However, geodynamic trigger of the Cretaceous continental-scale NW–SE extension in eastern Asia is still a mystery.

Keywords Dabieshan · HP–UHP orogenic belt · Extensional collapse · Metamorphic core complex · Crustal anatexis · Multiple detachments

Introduction

The Qinling–Tongbai–Dabie–Sulu orogenic belt between the North China block (NCB, the North China Craton or Sino-Korea Craton) and the South China block (SCB, comprising the Yangtze block in the northwest and the Cathaysia block in the southeast) was built by multistage orogeny from Paleozoic to Triassic (e.g., Mattauer et al. 1985; Meng and Zhang 2000; Ratschbacher et al. 2003, 2006; Dong et al. 2011; Wu and Zheng 2013; Dong and Santosh 2016). In particular, the finally Triassic continental deep subduction of the Yangtze plate beneath the NCB gave rise to the largest high-pressure and ultrahigh-pressure (HP–UHP)

✉ Wei Lin
linwei@mail.iggcas.ac.cn

Wenbin Ji
jiwenbin@mail.iggcas.ac.cn

[1] State Key Laboratory of Lithospheric Evolution, Institute of Geology and Geophysics, Chinese Academy of Sciences, Beijing 100029, China

[2] Institut des Sciences de la Terre d'Orléans, Université d'Orléans, 45071 Orléans, France

[3] School of Resource and Environment Engineering, Hefei University of Technology, Hefei 230009, China

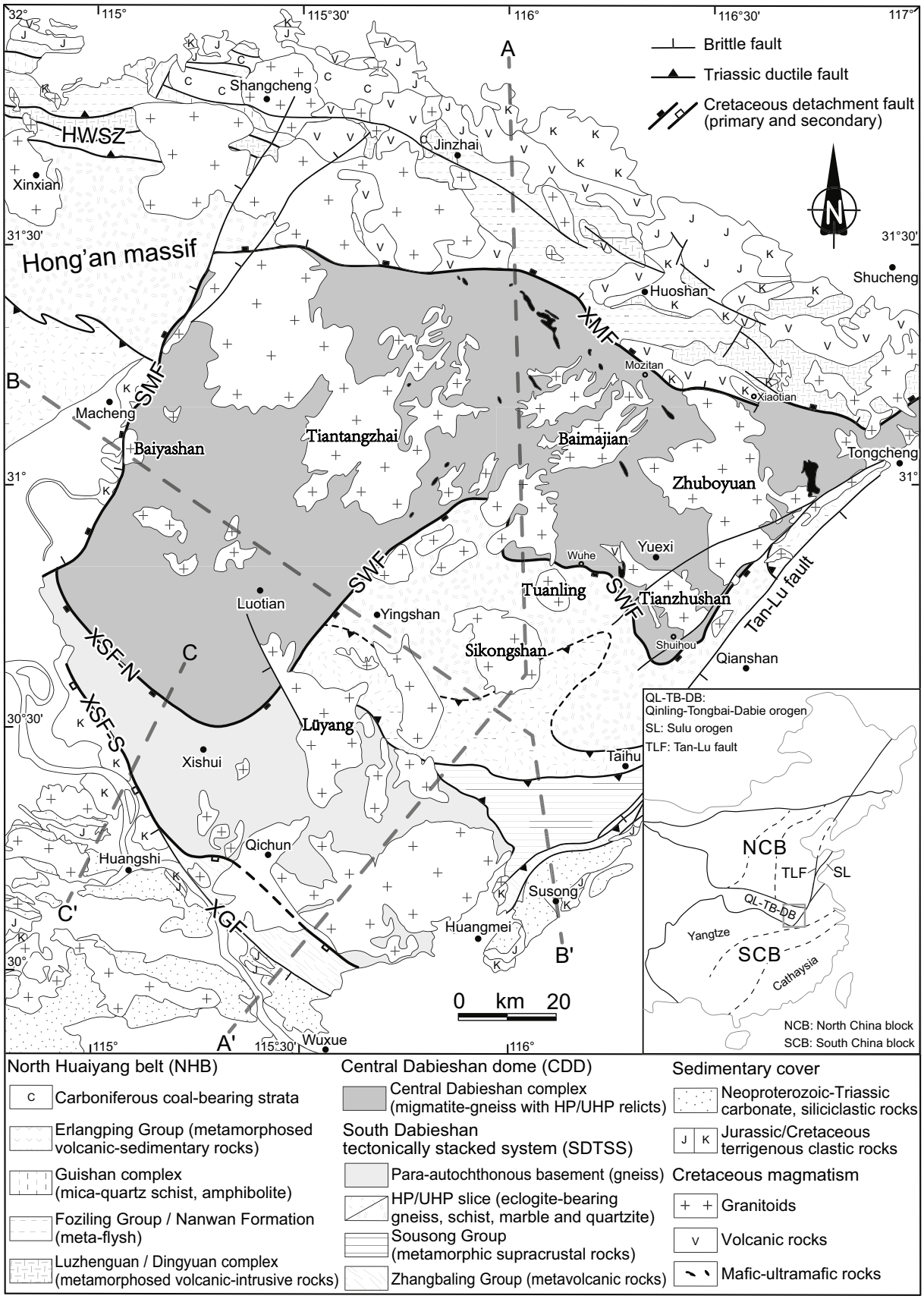
Brittle fault
Triassic ductile fault
Cretaceous detachment fault (primary and secondary)
N
Hong'an massif
HWSZ
SMF
XMF
SWF
XSF-N
XSF-S
XGF
Tan-Lu fault
Shangcheng
Xinxian
Jinzhai
Huoshan
Shucheng
Macheng
Baiyashan
Tiantangzhai
Baimajian
Zhuboyuan
Mozitan
Xiaotian
Tongcheng
Wuhe
Yuexi
Tianzhushan
Tuanling
Luotian
Yingshan
Sikongshan
Shuihou
Qianshan
Lüyang
Taihu
Xishui
Qichun
Huangshi
Susong
Huangmei
Wuxue
A
A'
B
B'
C
C'
0 km 20
115°
115°30'
116°
116°30'
117°
32°
31°30'
31°
30°30'
30°
QL-TB-DB:
Qinling-Tongbai-Dabie orogen
SL: Sulu orogen
TLF: Tan-Lu fault
NCB
SCB
TLF
SL
QL-TB-DB
Yangtze
Cathaysia
NCB: North China block
SCB: South China block
North Huaiyang belt (NHB)
C Carboniferous coal-bearing strata
Erlangping Group (metamorphosed volcanic-sedimentary rocks)
Guishan complex (mica-quartz schist, amphibolite)
Foziling Group / Nanwan Formation (meta-flysh)
Luzhenguan / Dingyuan complex (metamorphosed volcanic-intrusive rocks)
Central Dabieshan dome (CDD)
Central Dabieshan complex (migmatite-gneiss with HP/UHP relicts)
South Dabieshan tectonically stacked system (SDTSS)
Para-autochthonous basement (gneiss)
HP/UHP slice (eclogite-bearing gneiss, schist, marble and quartzite)
Sousong Group (metamorphic supracrustal rocks)
Zhangbaling Group (metavolcanic rocks)
Sedimentary cover
Neoproterozoic-Triassic carbonate, siliciclastic rocks
J K Jurassic/Cretaceous terrigenous clastic rocks
Cretaceous magmatism
Granitoids
V Volcanic rocks
Mafic-ultramafic rocks

◀ **Fig. 1** Geological map of the Dabieshan massif. *Inset* shows location of the massif within the Qingling–Tongbai–Dabie–Sulu orogenic belt in east-central China. Major faults: *XMF* Xiaotian-Mozitan fault, *SMF* Shangchang-Machang fault, *SWF* Shuihou-Wuhe fault, *XSF-N and XSF-S* north-Xishui fault and south-Xishui fault, *XGF* Xiangfan-Guangji fault

metamorphic terrane in the world. Since coesite/diamond-bearing eclogites were discovered in the Dabieshan massif (Okay et al. 1989; Wang et al. 1989; Xu et al. 1992), numerous multidisciplinary investigations have been devoted to formation and exhumation processes of the HP–UHP rocks in the Dabie–Sulu orogen over the past decades (for reviews, see Zheng 2008; Zhang et al. 2009; Liou et al. 2012).

It is generally accepted by structural geologists that the central domain of the Dabieshan massif exhibits as an extensional dome (e.g., Hacker et al. 1995, 2000; Wang and Yang 1996; Wang et al. 1998, 2011b; Zhong et al. 1999; Faure et al. 1999, 2003; Ratschbacher et al. 2000, 2006; Suo et al. 2000, 2005; Lin et al. 2003, 2005, 2015; Hou et al. 2007; Ji et al. 2011). Such a crust-scale domal architecture was detected by seismic reflection data (Wang et al. 2000a; Yuan et al. 2003). However, detailed geometry and kinematics, timing and formation mechanism of the central Dabieshan dome (CDD) and its contribution to exhumation of the Triassic HP–UHP rocks remains controversial. The CDD is bounded by the Xiaotian-Mozitan fault (XMF) in the north, the Shangcheng-Macheng fault (SMF) in the west and the Shuihou-Wuhe fault (SWF) in the southeast (Fig. 1). The migmatite–gneiss with HP–UHP relicts inside the CDD, namely the central Dabieshan complex, represents the exposed deep crustal rocks in the Dabieshan massif. Several models have been proposed to account for origin of the CDD. For example, Zhong et al. (1999) and Suo et al. (2000, 2005) proposed that the post-collisional framework of the whole Tongbai–Dabie orogen is similar to a MCC with multi-layer detachments formed during 200–170 Ma. Faure et al. (1999, 2003) and Lin et al. (2003) suggested that the CDD was initially developed by top-to-the-NW main deformation in response to syn-orogenic exhumation of the HP–UHP rocks, and then the Cretaceous magmatism reset most of the $^{40}Ar/^{39}Ar$ ages. By contrast, Wang et al. (1998) assumed that the central Dabieshan complex and the allochthonic HP–UHP slices in the hanging wall were juxtaposed together during the Early Cretaceous by a low-angle ductile normal shear zone (amount to the SWF), and ESE-directed lateral extrusion limited by boundary strike-slip faults was considered to be the driving mechanism of the Cretaceous structures. In agreement with the hypothesis of Hacker et al. (1995, 1998) that the CDD is a magmatic-structural dome, Ratschbacher et al. (2000) employed a rolling hinge-isostatic rebound model along the XMF to explain the asymmetric emplacement of the central Dabieshan complex under a NW–SE subhorizontal extension between 140 and 120 Ma. Recently, Wang et al. (2011b) presented structural analysis of the XMF and the SWF and argued that the formation process of the CDD was controlled by a top-to-the-NW shearing of these two shear zones during 143–132 Ma. According to our preliminary work, the boundary faults of the CDD (including the XMF, the SMF and the SWF) were all activated as Cretaceous detachment faults with consistently top-to-the-NW kinematics (Ji et al. 2011). Moreover, it must be firstly noticed that the main exhumation deformation of the HP–UHP slices on the southeastern flank of the Dabieshan massif was also characterized by a top-to-the-NW shearing, corresponding to the amphibolite facies retrogression (Hacker et al. 1995, 2000; Faure et al. 1999, 2003; Lin et al. 2003, 2009; Shi et al. 2014). Thus, it is critical to distinguish superposed structures with different ages but similar kinematics in the Dabieshan massif.

After the Triassic NCB–SCB collision, one of the notable tectonic events in eastern China is the so-called "destruction of the North China Craton". Geophysical and geochemical evidences show that at least 100-km-thick lithospheric mantle beneath the eastern NCB had been removed, and the physical and chemical nature of the lithospheric mantle had also been fundamentally transformed. Timing, scope, mechanism and geodynamic trigger of the cratonic destruction is still in hot debate (for reviews, see Menzies et al. 2007; Wu et al. 2008; Zhu et al. 2012b). Recent years, increasing studies have focused on the Late Mesozoic extensional structures developed in North China, especially metamorphic core complexes (MCCs) such as the Hohhot, Yunmengshan, Yiwulüshan, Liaonan or South Liaodong peninsula, Linglong and Xiaoqinling (e.g., Davis et al. 2002; Liu et al. 2005a, 2013b; Lin and Wang 2006; Lin et al. 2008, 2011, 2013; Davis and Darby 2010; Charles et al. 2011, 2012; Wang et al. 2011a, 2012b; Zhang et al. 2012; Zhu et al. 2015). MCCs as a typical signature of lithospheric extension have been attested to be crust-scale response to cratonic destruction by tectonic denudation of the deep crustal rocks. In this paper, we present new structural and geochronological data, and define the Cretaceous Dabieshan as an orogen-scale MCC accompanied by crustal anatexis. It is proposed that extensional collapse of the Triassic HP–UHP orogen during the Cretaceous shares the same tectonic setting as the destruction of the North China Craton. This contribution will not only improve our understanding on the Cretaceous reworking of the Dabie orogen, but also provide new insights into the geodynamic framework of the Late Mesozoic extensional tectonics in eastern Asia.

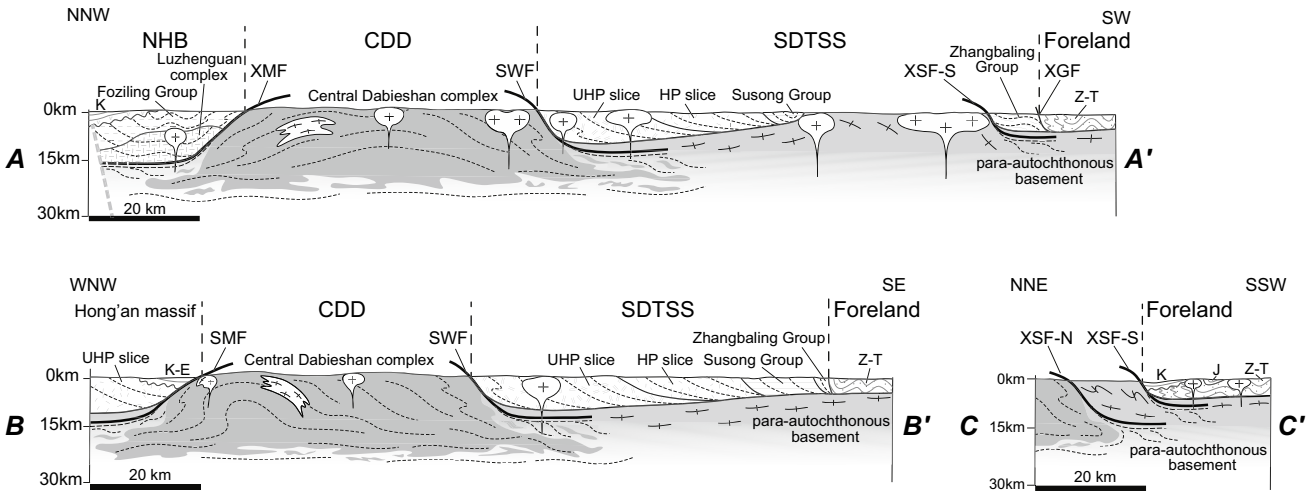

Fig. 2 Interpretative cross sections across the Dabieshan massif (see Fig. 1 for locations). Three domains: (1) *NHB* North Huaiyang belt, (2) *CDD* Central Dabieshan dome, (3) *SDTSS* South Dabieshan tectonically stacked system

Geological overview of the Dabieshan massif

The Dabie orogen is usually divided into two blocks by the SMF, namely the Hong'an massif in the west and the Dabieshan massif in the east (Fig. 1). The eastern end of the Dabieshan massif is truncated by the Tan-Lu fault that is generally believed as a continent-scale sinistral strike-slip fault in eastern China (Xu et al. 1987; Zhu et al. 2005; Zhao et al. 2016). Based on detailed fieldwork, we divide the Dabieshan massif into three domains from north to south (Faure et al. 1999, 2003; Lin et al. 2003, 2005; Ji et al. 2011): (1) the Beihuaiyang or North Huaiyang belt (NHB), (2) the Central Dabieshan dome (CDD, traditionally referenced to as the North Dabie) and (3) the South Dabieshan tectonically stacked system (SDTSS).

The NHB principally consists of the Foziling Group and the Luzhenguan complex (respectively, corresponding to the Nanwan Formation and the Dingyuan complex in the Hong'an massif), which experienced commonly greenschist facies locally up to amphibolite facies metamorphism (Figs. 1, 2). The Foziling Group is a suite of meta-flysch (mica-quartz schist, slate, phyllite, metasandstone and quartzite) deposited in the Devonian (Chen et al. 2003). Different investigators favored a passive continental margin or forearc setting for this flysch sequence (Okay et al. 1993; Xu et al. 2002b; Ratschbacher et al. 2006). The Luzhenguan complex is mainly composed of orthogneisses with minor amphibolites and schists, and their protoliths are mostly Neoproterozoic (780–750 Ma) volcanic-intrusive rocks related to rifting of the northern Yangtze margin (Chen et al. 2003; Zheng et al. 2004, 2007; Liu et al. 2013a). Besides, unmetamorphosed to weakly metamorphosed Carboniferous coal-bearing strata are partly survived in the Shangcheng area (Fig. 1). Zheng et al. (2005) regarded above low-grade metamorphic units in the NHB as an accretionary wedge that scraped off from the Yangtze plate during the Triassic continent subduction. Geometrically, the NHB constitutes a synclinorium with a smaller anticline in the central part. Due to relatively shallow subduction, polyphase deformation was preserved here, involving a top-to-the-S compressional deformation due to the plate convergence at ca. 260 Ma, and subsequent two-stages of exhumation deformation, respectively, with top-to-the-N/NE and top-to-the-NW shearing during the Middle and Late Triassic (Lin et al. 2005).

The CDD contains two sub-domes, namely the Luotian dome in the west and the Yuexi dome in the east (Figs. 1, 2). The central Dabieshan complex in the footwall consists of orthogneiss and subordinate amphibolite, marble, as well as rare granulite and eclogite. Variable extents of migmatization and associated amphibolite facies metamorphism are the pervasive features (Wang et al. 2002, 2013; Wu et al. 2007; Zhang et al. 2014; Chen et al. 2015). Unlike the South Dabieshan where HP–UHP eclogites are widespread; however, just rare UHP eclogites (as well as garnet-pyroxenites) overprinted by granulite facies retrogression have been identified in the CDD (Wei et al. 1998; Liu et al. 2000, 2005b, 2007a, 2011a, b; Tsai and Liou 2000; Xu et al. 2000, 2003; Malaspina et al. 2006; Groppo et al. 2015). Extraordinarily, several generations (possibly Paleoproterozoic, Triassic and Cretaceous) of granulites occur sparsely within the migmatitic gneisses (Zhang et al. 1996; Chen et al. 1998, 2006; Wu et al. 2008; Tong et al. 2011; Wang et al. 2012a; Jian et al. 2012). According to

petrology, geochemistry or geochronology, nature of the central Dabieshan complex has been variously interpreted as a metamorphosed ophiolitic mélange (Xu et al. 1992), a Paleozoic Andean-type magmatic arc complex (Zhai et al. 1994, 1995), a Triassic high-temperature metamorphic terrane that represents the Sino-Korean hanging wall (Zhang et al. 1996), a Cretaceous extensional-magmatic complex (Hacker et al. 1998, 2000; Ratschbacher et al. 2000), an extension of the Yangtze basement that was unaffected by the Triassic UHP metamorphism (Bryant et al. 2004) or a Triassic high-temperature/UHP terrane that belongs to part of the subducted Yangtze continent (Liu et al. 2007a, 2011a, b; Liu and Li 2008; Zheng 2008). Until now, it remains ambiguous that whether or not the entire central Dabieshan complex experienced the Triassic UHP metamorphic history (Tong et al. 2011).

The SDTSS contains several lithotectonic units separated by ductile faults. From bottom to top, the following units are recognized: (1) the para-autochthonous basement, (2) the HP–UHP slices, (3) the Susong Group and (4) the Zhangbaling Group (Figs. 1, 2). The para-autochthonous basement (also termed as the "UHP-free gneiss" by Faure et al. 1999, 2003 or the "Dabie complex" by Xu et al. 2002b, 2012c) consists of granitic gneiss, biotite/amphibole-plagioclase gneiss and minor amphibolite, representing part of the Yangtze basement that was not involved in the continental deep subduction. This unit only experienced amphibolite facies metamorphism and was less affected by the Cretaceous migmatization. We consider that the para-autochthonous basement was partially the precursor rocks of the migmatite in the CDD. The HP–UHP slices are composed of orthogneiss and paragneiss, interlayered with schist, marble and quartzite. Abundant eclogites occur as lenses, blocks or layers within the gneisses and marbles (e.g., Wang et al. 1992; Okay 1993; Carswell et al. 1997; Li et al. 2004; Shi and Wang 2006). Architecture of the HP–UHP slices has been recently reappraised by detailed structural and petrological work, and more pieces of HP rocks have been distinguished (Lin et al. 2009; Shi et al. 2014). A great number of studies have devoted to dating the eclogites and host-gneisses, showing that main phase of eclogite facies metamorphism occurred during 240–220 Ma, and their protoliths are mostly Neoproterozoic (820–740 Ma) igneous rocks with affinity of Yangtze plate (e.g., Ames et al. 1993, 1996; Li et al. 1993, 2000; Chavagnac and Jahn 1996; Rowley et al. 1997; Hacker et al. 1998; Chavagnac et al. 2001; Ayers et al. 2002; Li et al. 2004; Liu et al. 2006; Wawrzenitz et al. 2006; Wu et al. 2006). The Susong Group is a suite of epidote–amphibolite facies metamorphic supracrustal rocks with phosphorite deposit, comprising muscovite–albite gneiss, mica-quartz schist and marble. Blueschist–greenschist facies schist metamorphosed by acid to intermediate volcanic rocks is the dominant rock type of the Zhangbaling Group. Protoliths of the Susong and Zhangbaling Groups were also considered to be Neoproterozoic Yangtze crustal rocks, and experienced Triassic metamorphism (Xie et al. 2001a; Xu et al. 2002b, 2012c; Shi et al. 2012; Zhao et al. 2016). Structural features of these Triassic metamorphic sequences overlaying the para-autochthonous basement are commonly characterized by SE- to SSW-dipping foliations, NW–SE trending lineations and top-to-the-NW shearing (Hacker et al. 1995, 2000; Faure et al. 1999, 2003; Lin et al. 2003, 2009; Shi et al. 2014).

In the south front of the Dabieshan massif, Sinian (Late Neoproterozoic) to Middle Triassic marine carbonate and siliciclastic rocks, as well as Late Triassic and sporadically Jurassic terrigenous clastic rocks, comprise the sedimentary cover of the Yangtze foreland fold-thrust belt (Fig. 1). Cretaceous to Cenozoic basins filled with fluviatile and lacustrine deposits unconformably overlay the folded pre-Cretaceous strata. The Xiangfan-Guangji fault (XGF) is traditionally regarded as the boundary between the Yangtze foreland belt and the Tongbai–Dabie orogen. Seismic reflection data across the southern tip of the Dabieshan massif show that the Moho reflection beneath the XGF was segmented by several N-dipping thrusts (Dong et al. 2004). These Moho offsets probably represent remnants of the Early Mesozoic south-directed thrusting that was partly responsible for exhumation of the subducted Yangtze plate (Li et al. 2010; Yang et al. 2012). On the contrary, surface structures argue that the present XGF is a normal fault as suggested by Faure et al. (1999, 2003) and Lin et al. (2003).

An impressive feature of the Dabie orogen is the large-scale Cretaceous (143–117 Ma) magmatism, including voluminous granitoids and minor mafic–ultramafic rocks (Ma et al. 1998; Jahn et al. 1999; Chen et al. 2002; Zhao et al. 2004, 2005, 2007, 2011; Huang et al. 2007, 2008; Wang et al. 2007; Xu et al. 2007, 2012a, b; Zhang et al. 2010; He et al. 2011, 2013; Dai et al. 2012; Deng et al. 2014). Cretaceous granitoids occupy nearly half of the surface exposure of the Dabieshan massif (Fig. 1). The rock types of the granitoids mainly include monzonite, quartz monzonite, monzogranite and granite. According to geochronology and geochemistry, these granitoids can be grouped into two categories (e.g., Wang et al. 2007; Xu et al. 2007, 2012a, b; Huang et al. 2008; Zhang et al. 2010; He et al. 2011, 2013): (1) the early-stage (143–130 Ma) granitoids commonly display adakitic signatures (e.g., high Sr/Y and La/Yb ratios, low Y and HREE contents), which are interpreted to be derived from pre-existing thickened crust (>50 km); (2) the late-stage (younger than ca. 130 Ma) granitoids were derived from a normal crust, and therefore are defined as "normal granitoids." Small mafic–ultramafic intrusions (pyroxenite–gabbro) coeval with the late-stage granitoids are widely distributed in the CDD and

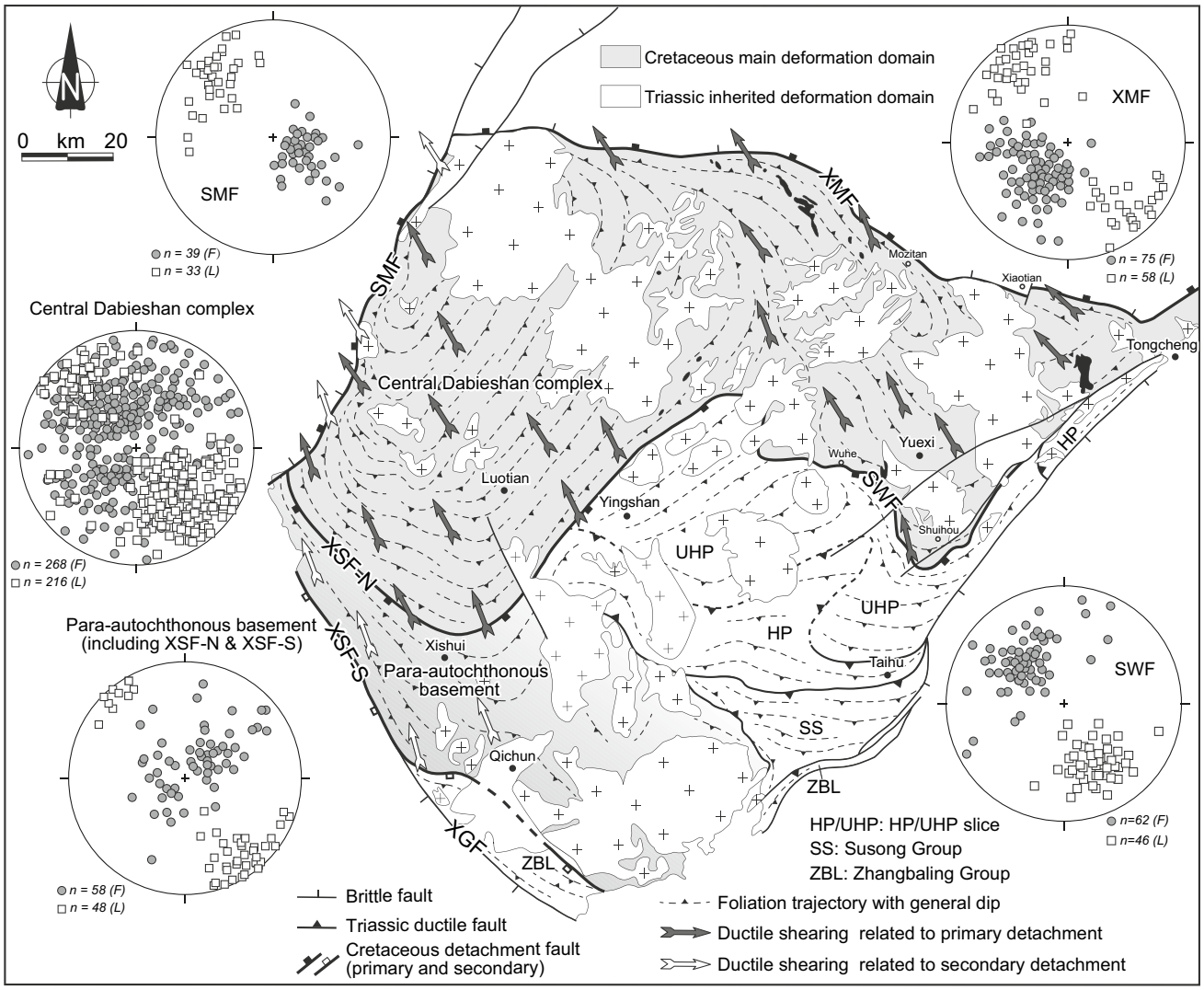

Fig. 3 Structural map of the Dabieshan MCC. All the stereographic diagrams are equal area, lower hemisphere projections of planar (F: foliation) and linear (L: lineation) structures

form several linear alignments (e.g., Jahn et al. 1999; Zhao et al. 2005; Huang et al. 2007; Dai et al. 2012). Additionally, there is also a Cretaceous volcanic belt that unconformably covers the low-grade metamorphic rocks of the NHB.

Structural analysis of the Dabieshan MCC

In this section, we present detailed structural analysis of the central Dabieshan complex in the footwall and the boundary faults of the CDD, as well as the southwestern Dabieshan margin (Figs. 2, 3). The central Dabieshan complex as footwall recorded distributed ductile deformation characterized by a NW–SE trending lineation and associated top-to-the-NW shearing. Overprinting of late brittle faulting makes we treat the XMF and the SMF as two individual faults. In fact, their early ductile components consistently with top-to-the-NW kinematics form a united but arched detachment fault along the northern and western boundaries of the CDD. The NHB to the north and the Hong'an massif to the west, as well as the supra-detachment Macheng half-graben basin, can be regarded as their hanging walls. Meanwhile, the SWF along the southeastern boundary of the CDD and the newly defined north-Xishui fault (XSF-N) and south-Xishui fault (XSF-S) in the southwestern Dabieshan margin probably constitute multiple detachment faults at different crustal levels. The Triassic metamorphic sequences as the hanging wall on the southeastern flank of the Dabieshan were dismembered by these SW- or SE-dipping detachments. Although their present kinematics appears to have thrust or strike-slip components in some

segments, if we restored them to originally subhorizontal attitude, their top-to-the-NW sense of shear is interpreted as extensional detachment. Such a pattern of detachment system is similar to that of the Hohhot MCC in Inner Mongolia described by Davis et al. (2002) and Davis and Darby (2010). In this case, the central domain of the Dabieshan massif is structurally defined as an orogen-scale MCC.

The central Dabieshan complex in the footwall

The CDD was occupied by migmatite–gneiss complex and granitic plutons. Two types of migmatite were distinguished in the CDD, namely diatexite and metatexite. Overall, diatexite is particularly abundant in the west-central part of the CDD, while metatexite is widely distributed in the whole CDD (Faure et al. 1999, 2003; Wang et al. 2002, 2013; Zhang et al. 2014). Field morphologies of the migmatite are commonly heterogeneous with various structures. The metatexite is characterized by stromatic structure, and it exhibits conspicuous foliation outlined by alternating compositional layers of leucosome and melanosome (Fig. 4a). Mafic layers were sometimes sheared into boudins, as a result, which made melt relocate to low-strain domains. This indicates that the deformation took place at high temperature while melt was still present in the rocks. Increasing extent of anatexis led progressive disaggregation of metatexite to form diatexite. Rafts or schollen of mafic blocks as restites are typical in metatexite–diatexite transition zone (Fig. 4b). Toward the diatexite domain, melt segregation give rise to schlieren consisting mostly of biotite, with minor amphibole and pyroxene. The migmatitic foliation in diatexite is generally marked by alignment of schlieren and mafic lens (Fig. 4c).

The foliation trajectories outline the geometrical patterns of the two subdomes (Fig. 3). The Luotian dome has an asymmetrically conchoidal shape with core approach to the SMF that cuts off mostly the western limb. The foliation dips to the NE and the SW, respectively, in the northeastern and southwestern limbs, and progressively turns into SE-dipping in the relatively broad southeastern limb. Large part of the Yuexi dome is intruded by granitic plutons, and as a result attitude of the foliation becomes relatively variable. The border between the two subdomes is unclear, except that a synformal structure in the north appears to separate them. In the gneissic or mylonitic migmatite along the dome margins, mineral and stretching lineations are overwhelming NW–SE trending (Fig. 3). These lineations are usually defined by recrystallized feldspars and quartz ribbons, biotite aggregates, and oriented crystals of amphibole (if present). Isoclinal folds with axes parallel to the lineation were also observed. Various shear sense indicators, including asymmetric folds, shear bands or S-C fabrics, asymmetric boudins (Fig. 4d) and sigma-type porphyroclasts of K-feldspar megacrysts (Fig. 4e), indicate that the deformation was dominated by a top-to-the-NW shearing (see also Hacker et al. 1995; Faure et al. 1999, 2003; Ji et al. 2011; Wang et al. 2011b). Toward the central part of the Luotian dome, structural patterns related to plastic flow of the partially molten crust become prevalent. There, lineation may be difficult to discern in the field due to high-temperature recrystallization. Nevertheless, along NW–SE transects, the transport direction is in general top-to-the-NW except for locally coaxial component. Thus, the migmatization in the CDD is a syn-tectonic process accompanied by crustal ductile deformation.

Cretaceous granitoids are widely distributed in the Dabieshan. There are several representative batholiths in the CDD, such as the Tiantangzhai, Baimajian, Zhuboyuan and Tianzhushan (Fig. 1). Field surveys show that the younger (after 130 Ma) granitic plutons such as the Baimajian batholith have isotropic structure without obvious deformation. By contrast, the granitic plutons emplaced during 143–130 Ma commonly exhibit solid-state or subsolidus deformation more or less. For example, early intrusions of the largest Tiantangzhi batholith in the Luotian dome developed gneissic or banded structure that can be traced into the migmatitic gneiss (Wang et al. 2007; Xu et al. 2007, 2012a; Deng et al. 2014). During our field survey, top-to-the-NW sense of shear indicated by augens of K-feldspar phenocrysts was observed in a small granitic stock to the northwest of Luotian (Fig. 4f). Due to similar mineral assemblage and deformation feature, sometimes it is difficult to unambiguously distinguish the border of the gneissic or anatectic granite from surrounding migmatite–gneiss complex in the field. Probably, some of the so-called Cretaceous gneisses dated by previous investigators are strongly foliated granites (Xue et al. 1997; Hacker et al. 1998; Bryant et al. 2004; Xie et al. 2006). Therefore, the early-stage granitoids in the CDD can be identified as syn-kinematic plutons coeval with the crustal detachment.

The XMF along the northern boundary of the CDD

The WNW-ESE trending XMF is limited between the SMF and the Tan-Lu fault (Fig. 1). The tectonic nature of this fault is controversial in geological evolution of the Dabieshan. In the "syn-exhumation extensional dome" model proposed by Faure et al. (1999, 2003) and Lin et al. (2003), the XMF together with the SMF was considered as an arched detachment related to the Triassic exhumation of the HP–UHP rocks, and then it was reactivated as a Cretaceous normal fault coeval with pluton emplacement. Hacker et al. (2000) and Ratschbacher et al. (2000) also suggested that the XMF is a polyphase fault: (1) Triassic detachment fault as the eastward prolongation of the Huwan shear zone in the northern Hong'an massif that facilitated the early

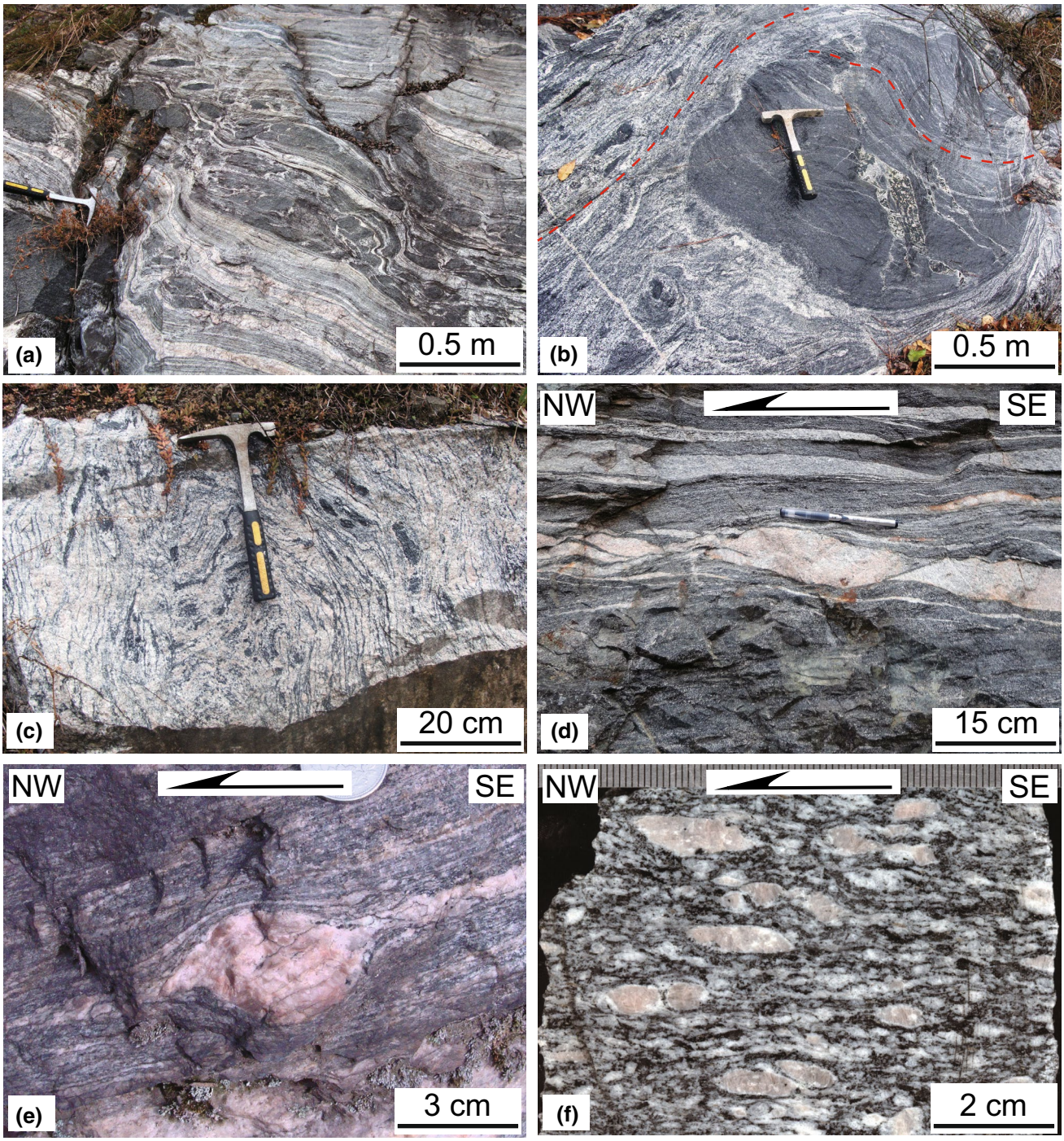

Fig. 4 Lithological and structural features of the Central Dabieshan complex. **a** Stromatic metatexite with gneissic foliation, note there are two types of leucosome: one is fine-grained with *light gray color*, while another is coarse-grained with *light pink color*. **b** Amphibolite block as restite within the migmatite, showing an internal foliation oblique to the migmatitic foliation. **c** Diatexite with folded leucosome and wispy layers of schlieren. **d** Asymmetric boudins of leucocratic vein within the gneiss indicate a top-to-the-NW sense of shear. **e** Sigma-type porphyroclast of K-feldspar megacryst in migmatitic gneiss indicates a top-to-the-NW sense of shear. **f** K-feldspar augens in a syn-kinematic granitic pluton show a top-to-the-NW sense of shear

exhumation of the HP–UHP rocks; (2) Early Cretaceous normal-sinistral or transtensional fault that controlled the exhumation geometry of the CDD; (3) 100–90 Ma dextral strike-slip fault conjugate to the sinistral Tan-Lu fault. Suo et al. (2000) speculated that the XMF represent the significantly reworked suture between the NCB and SCB. Wang

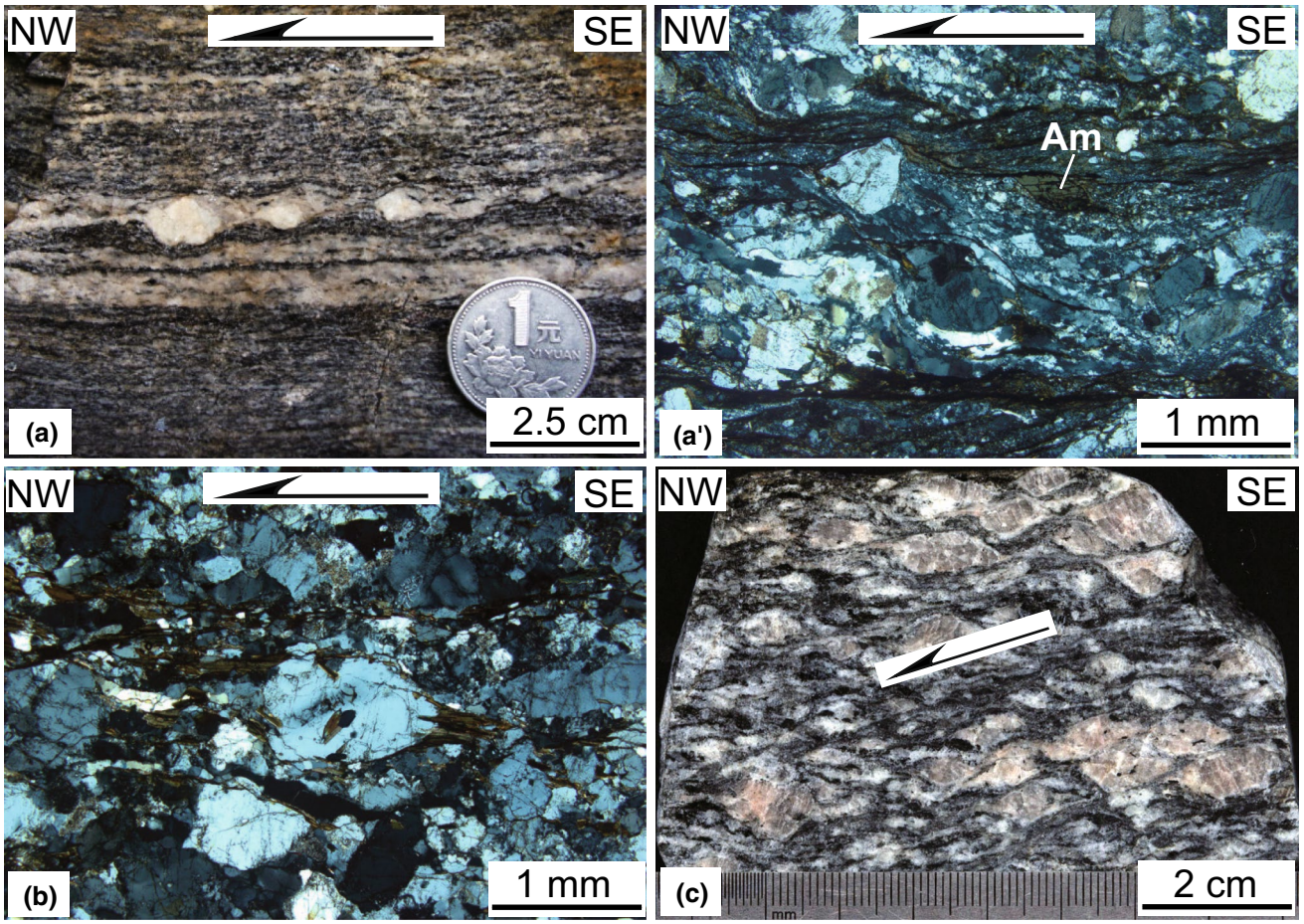

Fig. 5 Structural features of the XMF. **a** Sigma-type feldspar megacrysts at outcrop and **a′** amphibole (Am) mineral fish in thin-section of mylonitic migmatite (sample JS109). **b** Plagioclase porphyroclast with asymmetrical tail of biotite in mylonitic migmatite. **c** Syn-kinematic granitic pluton with augen structure and S-C fabrics. All *above* indicate a top-to-the-NW sense of shear

et al. (2011b) assumed that the XMF and the SWF were originally a single connected detachment zone developed at a middle crustal level before the Cretaceous doming. Nevertheless, seismic reflection data reveals that the XMF is an intra-crustal fault with north-dipping listric geometry, and there is a Moho offset beneath the XMF that was considered to be the plausible channel for continental deep subduction and exhumation (Yuan et al. 2003). Thus, the early history of the XMF, if any, had been completely erased.

The current XMF exhibits as a major detachment fault with ductile shear zone in deep portion overprinted by brittle fault in shallow portion. Protomylonite, mylonite, and locally ultramylonite of deformed migmatite–gneiss are well exposed along the middle and eastern segments of the XMF, and discontinuously distributed in the western segment due to the emplacement of granitic plutons. In different levels of the shear zone, mineral assemblages and microstructures of the tectonites indicate that the XMF experienced progressive deformation from amphibolite to greenschist facies conditions. The mylonitic foliation generally dips to the NE, with a low angle concentrated at 20°–45° (Fig. 3). On the conspicuous foliation, a NW–SE trending stretching lineation with shallow plunge is well developed. Shear sense indicators, such as S-C fabrics, asymmetric tails of feldspar porphyroclasts and mineral fish of amphibole, were observed either at outcrops or in oriented thin sections of mylonitic migmatite–gneiss (Fig. 5a, a′, b). Some granitic plutons close to the XMF were also involved into mylonitization, with augen structure and S-C fabrics (Fig. 5c). All above criteria consistently attested a top-to-the-NW sense of shear, as documented by previous authors (Faure et al. 1999, 2003; Ratschbacher et al. 2000; Lin et al. 2005, 2015; Ji et al. 2011; Wang et al. 2011b). A brittle normal fault zone with chloritized breccias separates the central Dabieshan complex in the footwall from the overlying low-grade metamorphic rocks as well as volcanic rocks in the hanging wall. Geometry of the slickensides and fault steps indicate a normal slipping. Infilling of the Cretaceous volcanic-clastic rocks in the Xiaotian basin was obviously controlled by activity of the XMF (Fig. 1).

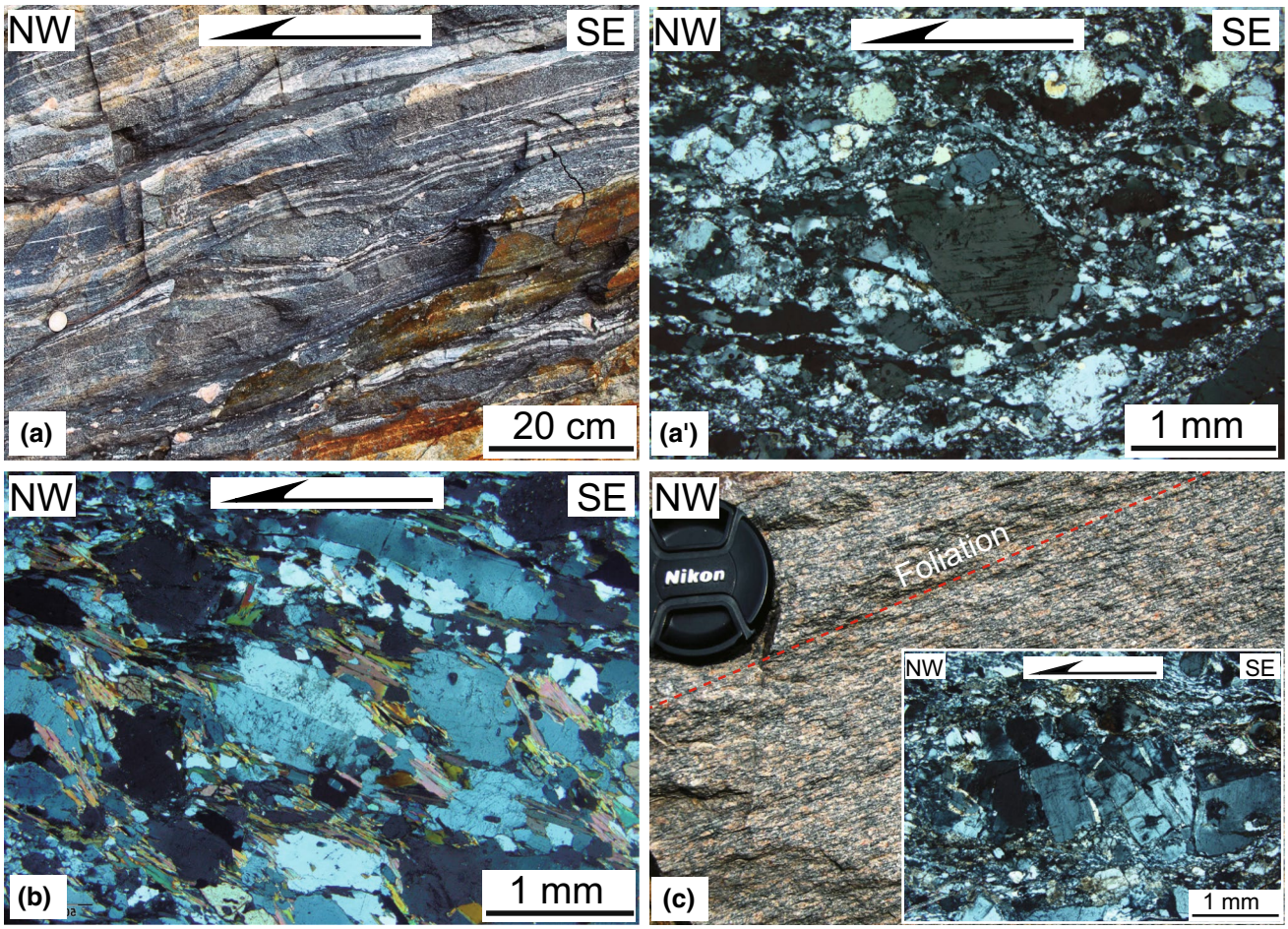

Fig. 6 Structural features of the SMF. **a** Sigmoid mafic lens within the mylonitic migmatite and **a′** sigma-type feldspar porphyroclast in thin section (sample DS49). **b** Sigma-type porphyroclast system in granitic mylonite (sample QD124). **c** Fragmented K-feldspar porphyroclast in mylonitic granite of the Baiyashan pluton. All above indicate a top-to-the-NW sense of shear

Furthermore, NE-vergent folds can be frequently observed in the Foziling meta-flysch at the north side of the XMF. This indicates gravity-driven décollement of the hanging wall accommodated to the doming. Such collapse-style folds can also be recognized in the SDTSS and Yangtze foreland belt, but with south-dipping axial planes (see also Faure et al. 1999, 2003; Lin et al. 2003, 2005).

The SMF along the western boundary of the CDD

The SMF strikes 20°–30° NE, and separates the Hong'an and Dabieshan massifs (Fig. 1). It also constitutes the boundary fault of the Late Cretaceous-Cenozoic Macheng half-graben basin to the west. However, the significant role of the SMF has always been ignored by previous models, such as lateral extrusion (Wang et al. 1998), rolling hinge-isostatic rebound (Ratschbacher et al. 2000), orogen-parallel extension of the ductile lithosphere (Wang et al. 2011b). Since only a few surveys have been conducted, origin of the SMF is poorly understood. Wang et al. (2000b) suggested that the SMF originated as a wrench fault during the Triassic collision and resulted in differential exhumation of the HP–UHP rocks in its two sides. On the other hand, ductile deformation related to Cretaceous extension has been recognized for the SMF (Wang et al. 2008; Ji et al. 2011).

Our detailed investigations on geometry and kinematics reveal that the SMF has a polyphase history similar to the XMF. Across the main fault zone, from east to west, the SMF is characterized by a gradual transformation from mylonitic to cataclastic rocks, and the deformation conditions also change from amphibolite facies to greenschist facies. This reveals a progressive exhumation process of the footwall from deep to shallow crustal levels. The mylonitic foliation dips gently at 15°–30° to the NW, where bears a NW–SE trending stretching lineation (Fig. 3). Kinematic indicators such as asymmetric boudins of mafic layer and sigma-type feldspar porphyroclasts in the mylonitic migmatite or granitic mylonite indicate a top-to-the-NW

shearing (Fig. 6a, a′, b). The brittle fault with high angle about 60°–85° cuts the early mylonitic foliation. Down-dipping slickenlines on fault surface show a normal motion with the west side moving downward. Moreover, eastward tilting of the red beds in the half-graben suggests that normal faulting of the SMF controlled the opening and infilling of the basin.

It is worth noted that at the middle segment of the SMF, the western margin of the Baiyashan pluton was involved in mylonitization (Figs. 1, 6c). The mylonitic granite exhibits a NW-dipping foliation with NW-plunging lineation. Under microscope, fragmented feldspar porphyroclasts attest a top-to-the-NW sense of shear. This kinematics is apparently consistent with ductile deformation of the SMF. However, microfabrics of the feldspar in the deformed granite are dominated by brittle fracturing and cataclastic flow, suggesting that the deformation temperature is below 400 °C. Such a feature is distinct from the relatively high-temperature (above 500 °C) subsolidus to solid-state deformation that extensively recorded in the migmatite–gneiss complex (see also Wang et al. 2011b). Meanwhile, the eastern part of this pluton exhibits massive structure without obvious solid-state deformation and has an intrusive contact with the deformed country rock. Thus, the SMF might experience at least two phases of ductile shearing, respectively, before and after emplacement of the Baiyashan pluton. This deduction is also supported by our $^{40}Ar/^{39}Ar$ dating results of tectonites from the SMF (see below).

The SWF along the southeastern boundary of the CDD

The contact between the HP–UHP slices and the underlying central Dabieshan complex is less well defined, because it is not a sharp boundary as the SMF and the XMF. According to Xu et al. (2002b) and our own fieldwork, this boundary can be roughly drawn (Figs. 1, 3). It originates from the east of Yuexi, passes through the Shuihou and Wuhe villages, then turns to the SW by way of Yingshan and Xishui, and finally terminated by the brittle SMF. Previous studies on this boundary were mainly concentrated at its eastern segment (the Yuexi-Yingshan area), where the SWF was named. Various patterns have been suggested for the SWF by different authors, such as a deep-seated thrust (Okay et al. 1993), the top boundary of the UHP terrain with a two-way movement (Wang et al. 1995), a Cretaceous ESE-directed low-angle ductile normal shear zone (Wang et al. 1998), local boundaries with normal or sinistral transtensive shear (Ratschbacher et al. 2000), and a Cretaceous top-to-the-NW shear zone (Ji et al. 2011; Wang et al. 2011b).

Field surveys show that the SWF usually occurs as a series of mylonitic zones alternated by weakly deformed domains, each of which ranges from tens to several hundred meters in width. West of Yingshan, NE-striking mylonitic zones parallel to each other distribute discontinuously both in the migmatite–gneiss complex and HP–UHP gneiss. Statistical result shows the mylonitic foliation of these high-strain zones dips predominantly to the SE with moderate to steep angles (about 30°–70°), and the lineation consistently plunges SE (about 130°–160°) (Fig. 3). Outcrop-scale shear bands in weakly migmatitic gneiss indicate a top-to-the-NW sense of shear (Fig. 7a). In the Wuhe-Shuihou segment, the SWF has a corrugated surface partly due to the disturbance of granitic plutons, and the mylonitic foliation locally dips steeply to the S or SSW (Fig. 3). In particular, quartz-feldspar mylonites characterized by strongly recrystallization were well exposed near the Shuihou town. Alignment of the biotite clots in some outcrops exhibits a pronounced NW–SE trending stretching lineation (Fig. 7b). Kinematic observations show a top-to-the-NW sense of shear, as attested by asymmetric pressure shadows surrounding feldspar porphyroclasts on hand specimen and mica fish under microscope (Fig. 7c, c′).

The newly defined XSF-N and XSF-S in the southwestern Dabieshan margin

Most authors assumed that there was a dextral strike-slip shear zone across the southwestern margin of the Dabieshan, which can extend even westward to the southern Tongbai orogen (Wang et al. 1998, 2003; Webb et al. 1999; Cui et al. 2012; Cheng et al. 2012; Zhao et al. 2016). Combined with the postulation that the XMF to the north is a coeval sinistral strike-slip boundary, SE-directed lateral extrusion of the whole Tongbai–Dabie orogen at sometime of the Mesozoic has been proposed. However, no evidence for regional-scale ductile strike-slip tectonics has been recognized by our structural investigations. Based on detailed mapping, we identified two detachment faults in the Xishui area, namely the XSF-N and the XSF-S (Figs. 1, 3). They occur as horsetail-like mylonite belts with two main branches. Speculatively, the XSF-N is the westward prolongation of the SWF, while the XSF-S partly reworked the XGF and detached the Zhangbaling Group in the southern tip of the Dabieshan.

The bulk architecture of the southwestern Dabieshan margin forms a southward arched structure accommodated to the geometry of the CDD (Fig. 3). Migmatization of the Central Dabieshan complex gradually disappeared into the para-autochthonous basement. This indicates that the pre-existing para-autochthonous basement situated in the central Dabieshan domain was partly involved in migmatization. The XSF-N and the XSF-S was mainly overprinted in the para-autochthonous basement, where the exposed gneisses were widely suffered mylonitization with pervasive planar and linear structures. Foliation trajectories in map view roughly trace the strikes of the XSF-N and the

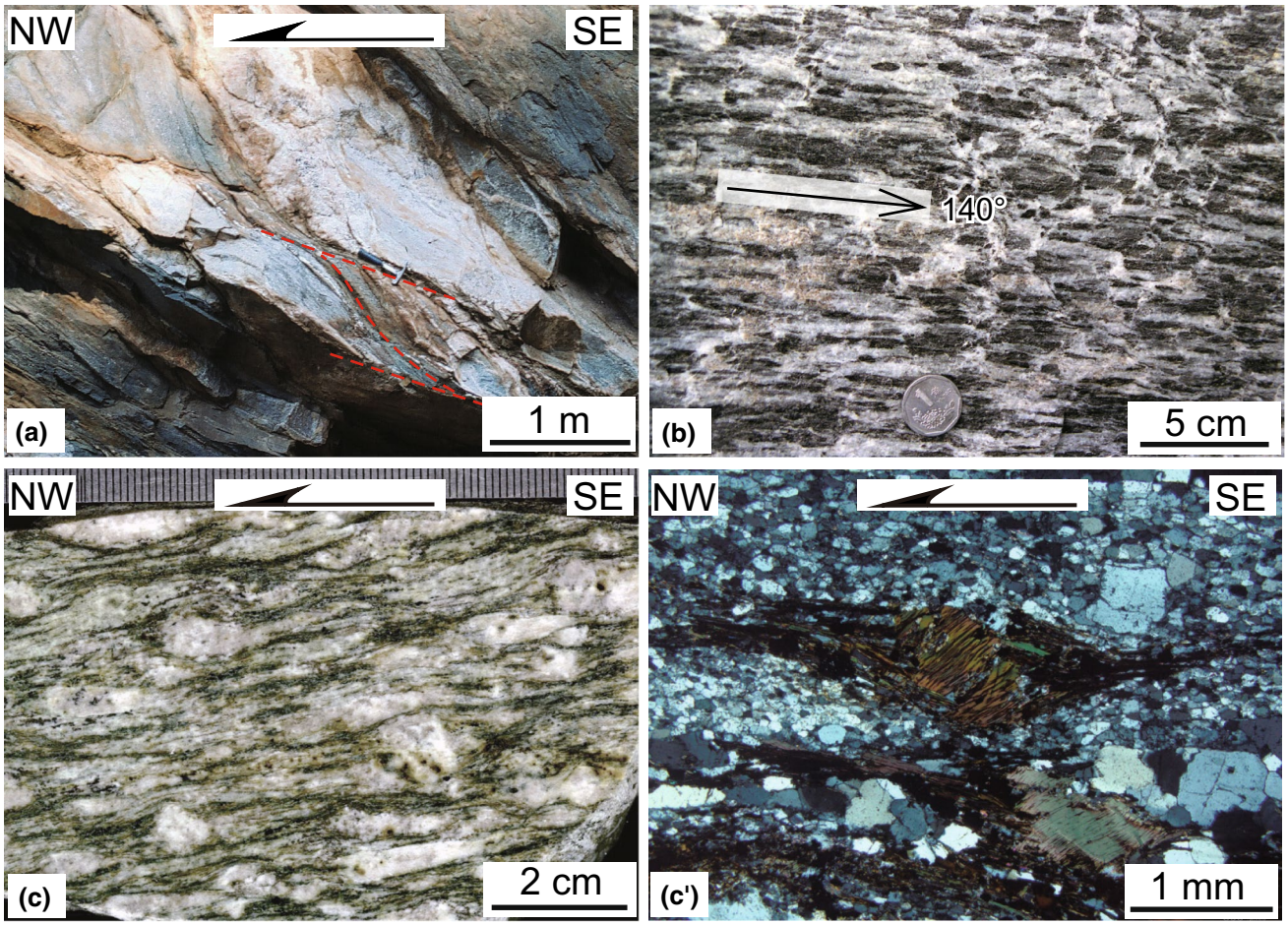

Fig. 7 Structural features of the SWF. **a** Outcrop-scale shear bands in migmatitic gneiss indicate a top-to-the-NW sense of shear. **b** Biotite clots in granitic mylonite constitute a NW–SE trending stretching lineation. **c** Sigma-type feldspar porphyroclasts and **c′** mica fish in granitic mylonite indicate a top-to-the-NW sense of shear (sample JS100)

XSF-S. West of Xishui, quartz-feldspar mylonites especially L-type tectonites are common since the XSF-N and the XSF-S converged there. The mylonitic foliations in this domain dip chiefly to the SW and subordinately to the NE, usually with low to moderate angles about 20°–50°. Along a NE–SW transect, unnegligible reverse of the attitudes reveals a series of folds with NW–SE trending axes. Whether the foliation is flat-lying or locally steep, the mineral stretching lineation keeps its NW–SE trend with subhorizontal or shallow plunges. This lineation is well defined by the elongation of feldspar porphyroclasts and development of quartz ribbons, as well as preferred alignment of biotite and epidote (Fig. 8a, b). Sigma-type feldspar porphyroclasts, sigmoid grains of quartz-feldspar and minor shear bands in orientated thin sections of the mylonitic rocks indicate a top-to-the-NW sense of shear (Fig. 8c–e). Thus, the lineation-parallel folds in the para-autochthonous basement are interpreted as isoclinal folds (i.e., A-type folds), developed by the principal NW–SE stretching (σ_1) accompanied by NE–SW contraction (σ_3). Although the XSF-N and the XSF-S have the same kinematics, the former rooted at a deeper crustal level than the latter in view of microstructures and deformation conditions (Fig. 2).

Geochronological constrains

Protolith and metamorphic ages of the central Dabieshan complex and timing of the migmatization

To constraint the protolith and metamorphic ages of the dominant orthogneisses in the CDD, a great deal of studies on zircon U–Pb dating have been performed. Initially, Xue et al. (1997) and Hacker et al. (1998) obtained U–Pb ages of 138–133 Ma from gneisses in the CDD, and interpreted these ages as the time of protolith emplacement. Bryant et al. (2004) subsequently identified three distinct types of gneisses, respectively, with protolith crystallization ages at

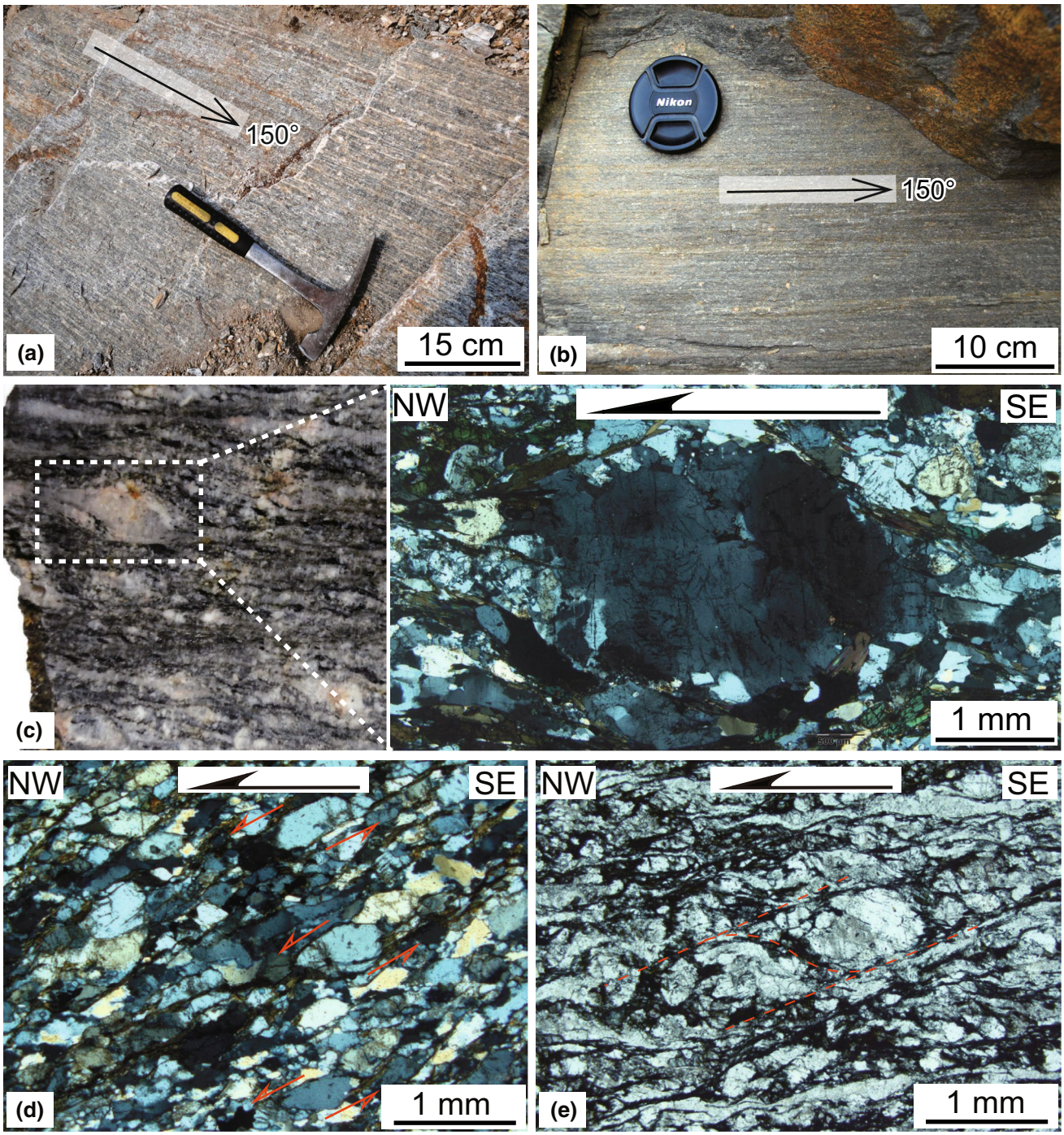

Fig. 8 Structural features of the southwestern Dabieshan margin. **a** NW–SE trending lineation in granitic mylonite of the XSF-N; **b** NW–SE trending lineation in biotite-plagioclase mylonite of the XSF-S; **c** Sigma-type K-feldspar porphyroclast in mylonite of the XSF-N indicate a top-to-the-NW sense of shear. **d** Sigmoid grains of plagioclase and quartz in mylonitic gneiss of the para-autochthonous basement indicate a top-to-the-NW sense of shear. **e** Minor shear bands in mylonite of the XSF-S indicate a top-to-the-NW sense of shear (sample DS45)

770 ± 26, 747 ± 14 and 127 ± 4 Ma, and inferred that the central Dabieshan complex was not affected by the Triassic UHP metamorphism. On the contrary, metamorphic zircons with TIMS weighted mean or lower intercept ages of 218–229 Ma from felsic gneisses at scattered locations in the CDD were reported by several investigators (Liu et al. 2000; Xie et al. 2001b; Jiang et al. 2002; Ge et al. 2003; Xue et al. 2003), evidently suggesting the presence

of Triassic metamorphism. By SHRIMP zircon U–Pb dating, Liu et al. (2007b) identified four different domains of zircons from two garnet-bearing tonalitic gneisses, comprising of 819 ± 15 Ma inherited core, 218 ± 3 Ma inner-mantle, 191 ± 5 Ma outer-mantle and 126 ± 5 Ma rim. The weighted mean age of 218 Ma therein on metamorphic zircon with diamond inclusion was regarded as the peak UHP metamorphic age. Zhao et al. (2008) also dated several granitic gneisses by TIMS, LA-ICPMS or SHRIMP, a weighted mean age of 751 ± 7 Ma calculated for all the dated samples was suggested as the protolith crystallization age, and two group ages of 245 ± 17–213 ± 4 and 131 ± 36–126 ± 4 Ma for regional metamorphism. Similarly, Xie et al. (2010) presented age groups of 760–730, 215–205, 138–137 and 124–120 Ma from three orthogneisses, corresponding to Neoproterozoic protolith formation, Triassic metamorphism and Cretaceous tectono-magmatism.

As a matter of fact, the so-called orthogneisses in the CDD comprise abundant migmatites. Wang et al. (2002) firstly dated a leucosome of the migmatite by TIMS technique, and the weighted mean age of 131.7 ± 1.1 Ma was regarded as the timing of migmatization. Wu et al. (2007) collected eight migmatite samples over a large area (including leucosome, melanosome and banded gneiss) for LA-ICPMS and SHRIMP zircon U–Pb dating. Four of them containing magmatic zircon cores yielded upper intercept ages of 807 ± 35–768 ± 12 Ma, suggesting that protoliths of the migmatites are Neoproterozoic in age; while all the metamorphic zircons yielded ages of 145 ± 2–120 ± 2 Ma with two major peaks at 139 and 123 Ma, indicating two episodes of partial melting. Recently, Wang et al. (2013) conducted SIMS zircon U–Pb dating for migmatites from the central part of the CDD, and the results gave three age cluster at 135, 130–132 and 128 Ma. They interpreted them as the earlier, peak and later melt crystallization time during the migmatization, respectively. Except for the 140–124 Ma anatectic event, Chen et al. (2015) further distinguished 200–192 Ma anatectic event, corresponding to "hot" exhumation of the UHP rocks and associated granulite facies overprinting.

In contrast to the SDTSS, occurrence of granulites and granulitized eclogites is one of the distinctive futures for the CDD. A mafic granulite from Huilanshan at the center of the Luotian dome was dated by both Sm–Nd and U–Pb methods (Hou et al. 2005). The mineral Sm–Nd isochron age of 136 ± 18 Ma was interpreted as the timing of granulite facies metamorphism, while the zircon cores with ages of 780–753 Ma were considered to be inherited from the Neoproterozoic protolith. The Huangtuling felsic granulite in the Luotian dome is well known as the oldest rock in the Dabieshan, which recorded ca. 2.0 Ga granulite facies metamorphism with protolith age at ca. 2.7 Ga (Wu et al. 2008; Jian et al. 2012). Furthermore, Wu et al. (2008) obtained a protolith age of 1982 ± 14 Ma for the host-gneiss of the Huangtuling granulite, and a few Cretaceous metamorphic zircon rims were also found from the gneiss. Based on a combined study of mineral inclusions, U–Pb ages and trace elements of zircons from several granulitized eclogites in the Luotian dome, Liu et al. (2011b) suggested a multi-stage metamorphic history with prograde metamorphism at 238 ± 2 Ma, UHP and HP eclogite facies metamorphism at 226 ± 3 and 214 ± 3 Ma, granulite facies and amphibolite facies retrograde metamorphism at 199 ± 2 and 176–188 Ma. Wang et al. (2012a) also recognized polyphase metamorphic zircons from a calc-silicate granulite in the eastern part of the CDD, and confirmed three episodes of metamorphism at 224 ± 2, 213 ± 2 and 200 ± 3 Ma that were interpreted as the timing of UHP eclogite facies metamorphism, granulite facies and amphibolite facies retrogressions, respectively.

Collectively, available zircon U–Pb geochronological data from the central Dabieshan complex usually give age associations of Neoproterozoic (820–740 Ma), Triassic (238–200 Ma) and/or Cretaceous (145–120 Ma). It is now generally accepted that the protoliths of the central Dabieshan complex are similar to that of the HP–UHP rocks in the SDTSS and the Luzhenguan complex in the NHB, in agreement with the Neoproterozoic rifting-related magmatism along the northern Yangtze margin. The Triassic ages undoubtedly represent the timing of metamorphism related to continental collision, while the Cretaceous ages are coeval with the crustal anatexis and magmatism during extensional collapse. Recent SIMS U–Pb dating on rutile in the eclogites from the CDD yielded Cretaceous ages, with a narrow span of 130–127 Ma (Li et al. 2013c; Lin et al. 2015). This result reveals that these Triassic eclogites experienced a protracted stagnation at a deep crustal level (above the closure temperature of rutile U–Pb system) before ca. 130 Ma. Moreover, almost the $^{40}Ar/^{39}Ar$ ages (amphibole and mica) from the migmatite–gneiss complex and granitic plutons in the CDD fall into a range from 142 to 100 Ma (Fig. 9) (Chen et al. 1991, 1995; Mattauer et al. 1991; Eide et al. 1994; Hacker and Wang 1995; Ratschbacher et al. 2000; Wang et al. 2002, 2011b; Xu et al. 2002a; Ma et al. 2004; Zhu et al. 2005; Hou et al. 2007; Lin et al. 2007, 2015). These ages are evidently related to the Early Cretaceous tectono-thermal event.

Geochronology of the detachment faults

Previous geochronological data

Previous geochronological data on detachment faults of the Dabieshan MCC mainly focused on the XMF, and direct $^{40}Ar/^{39}Ar$ dating of tectonites from other detachment

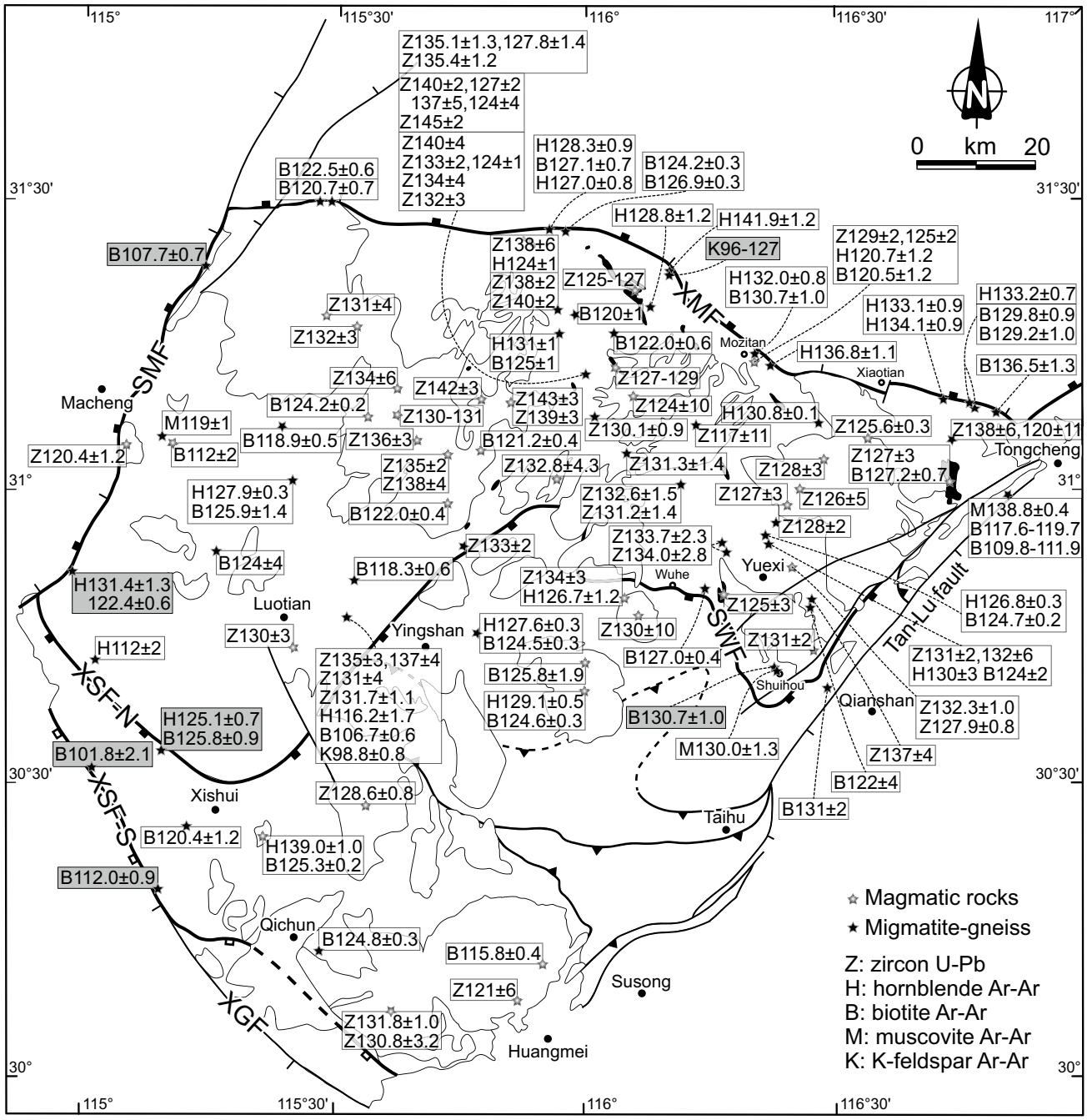

Fig. 9 Compilation of available geochronological data (U–Pb and $^{40}Ar/^{39}Ar$) related to the Early Cretaceous tectono-thermal event in the Dabieshan area. Data sources from (Chen et al. 1991, 1995, 2009; Mattauer et al. 1991; Eide et al. 1994; Hacker and Wang 1995; Xue et al. 1997; Hacker et al. 1998; Ratschbacher et al. 2000; Wang et al. 2002, 2011b, 2013; Xu et al. 2002a; Ma et al. 2004; Zhao et al. 2004, 2005, 2007, 2008, 2011; Zhu et al. 2005; Hou et al. 2007; Lin et al. 2007, 2015; Wu et al. 2007, 2008; Xie et al. 2010; He et al. 2011; Yang et al. 2012; Dai et al. 2012; Deng et al. 2014); this study (*gray box*)

faults is rare (Fig. 9). Hou et al. (2007) reported two biotite $^{40}Ar/^{39}Ar$ age of 124.2 ± 0.3 and 126.9 ± 0.3 Ma from tectonites in the eastern segment of the XMF. Wang et al. (2011b) presented abundant (more than ten) hornblende and biotite $^{40}Ar/^{39}Ar$ ages from mylonites along the XMF. The hornblende samples yielded ages ranging from 141.9 ± 1.2 to 127.0 ± 0.8 Ma, while the biotite samples from 130.7 ± 1.0 to 120.7 ± 0.7 Ma. In addition, a gabbro near Mozitan weakly deformed by the XMF yielded zircon U–Pb ages of 125 ± 2 Ma (TIMS) and 129 ± 2 Ma (SHRIMP), as well as hornblende and biotite $^{40}Ar/^{39}Ar$ ages of 120.7 and 120.5 Ma, respectively (Hacker et al. 1998;

Ratschbacher et al. 2000). Wang et al. (2000b) dated a biotite-plagioclase mylonite from the SMF, and the biotite age of 226.5 ± 0.6 Ma was considered as the onset time of the SMF. However, according to zircon U–Pb dating of a syn-kinematic pegmatite vein (with boudinage structure) and a post-kinematic granitic intrusion (cut the shear zone), Wang et al. (2008) argued that the transition time from ductile to brittle for the SMF can be constrained between 126 and 119 Ma. Our field survey shows that the Baiyashan pluton was partly involved in ductile shearing. Emplacement age of this pluton was dated at 120.4 ± 1.2 Ma by LA-ICPMS zircon U–Pb method (Figs. 1, 9) (Chen et al. 2009). That is, there was still localized shearing along the SMF after ca. 120 Ma. Ratschbacher et al. (2000) obtained muscovite and biotite $^{40}Ar/^{39}Ar$ ages of 130.0 ± 1.3 and 131 ± 2 Ma from two UHP paragneisses along the Qianshan-Yuexi transect, indicating that the Cretaceous activity of the SWF partly involved the UHP slice in the hanging wall. Moreover, the weakly deformed Tuanling tonalite at the south side of the SWF yielded a zircon U–Pb age of 134 ± 4 Ma and a hornblende $^{40}Ar/^{39}Ar$ age of 126.7 ± 1.2 Ma (Figs. 1, 9) (Hacker et al. 1998; Ratschbacher et al. 2000). Instead, Hou et al. (2007) reported a biotite age of 190.6 ± 0.4 Ma from tectonite in the Shuihou area and considered the SWF might contribute to exhumation of the UHP rocks, but the $^{40}Ar/^{39}Ar$ data and detailed description of the dated sample were not presented. Thus, both the SMF and the SWF record the Cretaceous tectono-thermal event, the two Early Mesozoic ages reported by Wang et al. (2000b) and Hou et al. (2007) require reappraisal.

New $^{40}Ar/^{39}Ar$ dating

Minerals including hornblende, biotite and K-feldspar in mylonites or mylonitic rocks from the detachment faults were separated for $^{40}Ar/^{39}Ar$ dating (sample locations see Fig. 9). The samples were irradiated in the reactor at Institute of Atomic Energy, Beijing. Thereafter, the $^{40}Ar/^{39}Ar$ analyses were performed using a MM-5400 mass spectrometer in Institute of Geology and Geophysics, Chinese Academy of Sciences (IGGCAS). Detailed sample processing and analytical procedures were described by Wang et al. (2014). Data calculation was processed by the ArArCALC software (Koppers 2002). The $^{40}Ar/^{39}Ar$ analytical data are listed in Table 1, their age spectra and reverse isochron plots are shown in Fig. 10. All age errors are reported at 2σ.

Since there are plenty of $^{40}Ar/^{39}Ar$ ages along the XMF, only one mylonite JS109 from the middle segment of the XMF has been dated in this study (Fig. 5a, a′). The K-feldspar age spectrum of this sample shows slightly increasing steps with apparent ages ranging from 96.5 to 127.6 Ma. In order to reveal the detailed cooling history of this sample between 350 and 150 °C, we carried out a multi-diffusion domain (MDD) modeling. The result indicated two phases of cooling during 130–115 Ma and after ca. 95 Ma, respectively (Fig. 10). We collected two samples from different locations along the SMF. Hornblende in a mylonitic migmatite DS49 (Fig. 6a, a′) from the southern segment of the SMF yielded a stair-shaped spectrum, dropping down from low to high temperature with ages of 131.4, 126.5 and 122.4 Ma. The weighted mean age of 131.4 ± 1.3 Ma therein calculated using three low-temperature steps is in accord with the inverse isochron age of 130.9 ± 1.4 Ma. Biotite in a granitic mylonite QD124 (Fig. 6b) from the northern segment of the SMF yielded a plateau age of 107.7 ± 0.7 Ma.

Sample JS100 is a granitic mylonite near the Shuihou town, showing a top-to-the-NW sense of shear (Fig. 7c, c′). Syn-kinematic biotite from this sample yielded a plateau age of 130.7 ± 1.0 Ma. Hornblende and biotite had been separated from the sample JS349, a mylonitic gneiss taken from the XSF-N. The more consistent high-temperature steps of the hornblende spectrum for JS349 yielded a weighted mean age of 125.1 ± 0.7 Ma and an inverse isochron age of 124.8 ± 1.0 Ma, while the biotite yielded a plateau age of 125.8 ± 0.9 Ma. Two samples DS39 and DS45 (Fig. 8e) are mylonites from the XSF-S, their biotite age spectra show concave-upward shapes, respectively, with total fusion age of 106.1 ± 0.8 and 96.6 ± 0.6 Ma. Although there is some collapse at middle steps of the spectrum for DS39, other flatter steps yielded a weighted mean age of 112.0 ± 0.9 Ma that agrees well with the inverse isochron age of 112.8 ± 2.6 Ma. Moreover, the $^{40}Ar/^{36}Ar$ intercept at 292.3 ± 9.8 is nearly equal to the atmospheric value. Similarly, a weighted mean age of 101.8 ± 2.1 Ma was calculated for DS45, corresponding to an inverse isochron age of 103.0 ± 6.7 Ma.

Timing of the detachment faults

The previously published $^{40}Ar/^{39}Ar$ dating results from the XMF fall into a slightly wide range of 142–120 Ma (Hou et al. 2007; Wang et al. 2011b). By and large, the hornblende ages (142–127 Ma) are older than the biotite ages (131–120 Ma), in accordance with the variation in closure temperatures of hornblende (about 500 °C) and biotite (about 300 °C). Since there is palingenetic hornblende in mylonite of the XMF, the hornblende ages are therefore closer to timing of the shear zone. Ductile shearing along the XMF probably activated as early as the oldest hornblende age of 142 Ma. As mentioned before, the SMF probably experienced two phases of ductile shearing before and after ca. 120 Ma. Thus, it is speculated that our two biotite ages of 131 Ma (DS49) and 108 Ma (QD124), respectively, recorded cooling related to the early and late ductile shearing along the SMF.

Table 1 $^{40}Ar/^{39}Ar$ analytical data of tectonites from detachment faults of the Dabieshan MCC

Temperature (°C)	$^{40}Ar/^{39}Ar$	$^{37}Ar/^{39}Ar$	$^{36}Ar/^{39}Ar$	$^{40}Ar^*/^{39}Ar$	$^{40}Ar^*$ (%)	^{39}Ar (%)	Age ± 2σ (Ma)
JS109, K-feldspar, $J = 0.004878$, GPS: 31°21′32″N; 116°10′54″E							
750	27.329	0.00434	0.05448	11.231	41.10	0.57	96.45 ± 2.70
770	15.901	0.00945	0.01285	12.105	76.13	1.60	103.75 ± 0.80
790	14.577	0.00959	0.00698	12.516	85.86	1.05	107.16 ± 0.70
820	14.807	0.00478	0.00527	13.251	89.49	1.41	113.27 ± 0.71
850	14.867	0.00590	0.00395	13.701	92.16	1.88	116.99 ± 0.67
870	15.056	0.00789	0.00408	13.852	92.00	1.70	118.24 ± 0.68
900	15.564	0.00344	0.00492	14.109	90.65	1.85	120.36 ± 0.61
930	15.797	0.00293	0.00560	14.143	89.53	1.80	120.64 ± 0.68
960	15.587	0.00473	0.00531	14.018	89.93	1.69	119.61 ± 0.66
1000	15.969	0.00658	0.00598	14.202	88.93	2.69	121.13 ± 0.60
1030	16.182	0.00406	0.00636	14.303	88.39	3.01	121.96 ± 0.60
1060	16.112	0.00381	0.00560	14.456	89.72	5.51	123.22 ± 0.57
1090	15.656	0.00310	0.00373	14.554	92.96	7.67	124.03 ± 0.54
1120	15.580	0.00107	0.00336	14.587	93.63	6.80	124.30 ± 0.54
1150	15.583	0.00048	0.00341	14.576	93.54	6.43	124.21 ± 0.57
1180	15.653	0.00170	0.00321	14.705	93.95	7.21	125.27 ± 0.53
1220	15.733	0.00156	0.00319	14.791	94.01	13.45	125.98 ± 0.57
1250	15.735	0.00182	0.00305	14.834	94.27	14.09	126.33 ± 0.60
1280	15.876	0.00199	0.00301	14.986	94.39	10.50	127.58 ± 1.93
1310	15.811	0.00022	0.00313	14.887	94.15	5.20	126.76 ± 0.58
1340	15.879	0.00038	0.00319	14.936	94.07	2.76	127.18 ± 1.89
1400	15.898	0.00423	0.00348	14.870	93.53	1.13	126.63 ± 0.73
QD124, Biotite, $J = 0.003344$, GPS: 31°22′39″N; 115°12′46″E							
750	19.114	3.03117	0.00317	18.467	96.36	6.09	108.36 ± 1.75
800	19.275	2.19618	0.00364	18.407	95.32	10.42	108.02 ± 1.29
840	19.123	1.66138	0.00327	18.313	95.63	12.45	107.48 ± 1.01
880	18.942	1.62326	0.00229	18.419	97.11	14.84	108.09 ± 0.92
910	18.700	1.57124	0.00178	18.324	97.86	12.78	107.54 ± 1.11
950	18.656	2.30802	0.00157	18.412	98.50	11.53	108.05 ± 1.07
990	18.429	2.18877	0.00153	18.185	98.49	10.02	106.75 ± 1.12
1030	18.486	2.67502	0.00134	18.344	99.01	8.50	107.66 ± 1.13
1070	19.335	3.01692	0.00144	19.197	99.03	7.33	112.51 ± 2.14
1110	18.484	4.89041	0.00172	18.440	99.35	6.05	108.21 ± 1.88
DS49, Hornblende, $J = 0.004800$, GPS: 30°52′38″N; 114°59′20″E							
820	178.163	0.74732	0.56871	10.177	5.71	0.61	86.25 ± 28.43
900	59.836	2.93355	0.14804	16.366	27.28	3.94	136.75 ± 5.85
1000	23.257	3.24219	0.02685	15.623	66.99	9.68	130.76 ± 1.71
1030	18.584	3.26131	0.01078	15.701	84.25	14.09	131.39 ± 0.89
1060	16.557	3.29705	0.00560	15.207	91.59	13.41	127.40 ± 0.63
1090	15.595	3.20449	0.00316	14.955	95.64	13.57	125.36 ± 0.62
1120	16.453	3.33774	0.00556	15.118	91.62	5.56	126.68 ± 0.68
1180	15.459	3.23841	0.00393	14.595	94.15	38.90	122.44 ± 0.60
1240	10.245	0.54089	0.01570	5.654	55.16	0.25	48.42 ± 6.43
JS100, Biotite, $J = 0.004811$, GPS: 30°42′31″N; 116°23′31″E							
750	28.508	0.02090	0.04855	14.162	49.68	2.13	119.19 ± 2.24
800	17.665	0.00108	0.00968	14.803	83.80	12.70	124.40 ± 0.69
820	19.468	0.00233	0.01368	15.426	79.24	8.80	129.45 ± 0.88
860	22.010	0.00473	0.02105	15.790	71.74	8.32	132.40 ± 1.05
900	18.191	0.00395	0.00898	15.538	85.41	6.30	130.36 ± 0.87

Table 1 continued

Temperature (°C)	$^{40}Ar/^{39}Ar$	$^{37}Ar/^{39}Ar$	$^{36}Ar/^{39}Ar$	$^{40}Ar^*/^{39}Ar$	$^{40}Ar^*$ (%)	^{39}Ar (%)	Age ± 2σ (Ma)
940	24.962	0.01145	0.03153	15.645	62.67	4.79	131.23 ± 1.45
980	24.995	0.02230	0.03037	16.024	64.11	5.50	134.29 ± 1.40
1020	18.113	0.02104	0.00866	15.556	85.88	12.48	130.51 ± 0.67
1040	16.470	0.00279	0.00357	15.414	93.59	13.73	129.36 ± 0.65
1060	16.350	0.00368	0.00270	15.551	95.12	12.14	130.47 ± 0.68
1080	16.391	0.00443	0.00277	15.574	95.02	7.19	130.65 ± 0.62
1120	16.751	0.03306	0.00321	15.806	94.35	3.88	132.53 ± 0.73
1160	16.297	0.06927	0.00297	15.424	94.64	1.57	129.44 ± 1.49
1260	20.923	0.12848	0.01801	15.612	74.61	0.46	130.97 ± 2.32
1300	57.595	0.02939	0.09128	30.632	53.18	0.03	248.59 ± 29.16
JS349, Hornblende, $J = 0.004848$, GPS: 30°32′08″N; 115°10′03″E (Bioltite data cf. Lin et al. 2015)							
880	364.219	3.26111	1.21790	4.606	1.26	0.26	39.93 ± 77.21
960	83.773	4.68072	0.20608	23.344	27.75	0.72	193.87 ± 47.48
1040	18.954	3.07878	0.01422	15.037	79.12	10.79	127.24 ± 1.32
1040	18.637	3.04580	0.01411	14.748	78.93	10.91	124.88 ± 3.97
1070	15.413	3.05483	0.00475	14.290	92.47	39.96	121.12 ± 0.74
1090	15.300	2.96173	0.00267	14.784	96.38	12.49	125.18 ± 0.60
1120	16.658	3.14146	0.00716	14.832	88.80	1.94	125.57 ± 0.85
1170	15.366	3.02222	0.00303	14.749	95.74	17.28	124.89 ± 0.60
1190	15.968	3.09543	0.00505	14.760	92.19	5.13	124.97 ± 0.82
1250	19.242	3.38351	0.02225	12.973	67.23	0.52	110.29 ± 2.83
DS39, Biotite, J = 0.004768, GPS: 30°20′21″N; 115°08′12″E							
750	67.244	0.00757	0.17596	14.166	22.68	15.25	126.92 ± 7.46
800	25.795	0.00520	0.04266	14.381	51.13	13.19	110.28 ± 1.91
830	20.319	0.00276	0.02311	14.817	66.40	13.49	112.73 ± 1.21
860	21.734	0.00673	0.02825	15.121	61.59	13.39	111.88 ± 1.30
900	35.610	0.01007	0.08010	15.201	33.53	11.94	100.13 ± 4.42
940	29.419	0.01554	0.06309	14.967	36.64	10.78	90.62 ± 2.65
980	20.505	0.00927	0.03139	14.721	54.77	11.23	94.33 ± 1.37
1010	20.434	0.00421	0.02612	14.831	62.22	12.71	106.43 ± 1.23
1040	22.009	0.00570	0.02916	14.924	60.85	13.39	111.94 ± 1.35
1080	33.718	0.05062	0.06845	15.004	40.02	13.49	112.76 ± 3.14
1180	413.600	4.17601	1.11794	15.109	20.21	83.89	608.44 ± 88.13
DS45, Biotite, J = 0.004791, GPS: 30°30′38″N; 115°02′43″E							
750	24.778	0.00484	0.04649	11.042	44.57	5.81	93.22 ± 2.00
800	16.265	0.00502	0.01449	11.983	73.68	23.51	100.95 ± 0.77
830	19.123	0.00819	0.02274	12.404	64.87	10.30	104.39 ± 1.04
870	24.990	0.01950	0.04541	11.574	46.32	7.97	97.59 ± 1.86
910	19.758	0.01180	0.03236	10.196	51.61	8.19	86.24 ± 1.36
950	19.169	0.01580	0.03132	9.917	51.73	12.09	83.94 ± 1.32
990	18.381	0.00813	0.02549	10.848	59.02	14.87	91.63 ± 1.12
1030	18.273	0.00845	0.02079	12.129	66.38	10.32	102.14 ± 1.01
1070	16.667	0.01857	0.01310	12.799	76.79	5.76	107.62 ± 0.84
1110	18.155	0.14641	0.01495	13.750	75.77	1.02	115.37 ± 1.51
1210	41.303	0.83237	0.09882	12.179	29.55	0.16	102.55 ± 21.36

The biotite age of 131 Ma from the Shuihou mylonite (JS100) was considered to be a good estimate for cooling age of the SWF. Some UHP rocks in the hanging wall of the SWF also yielded synchronous ages of 130–131 Ma (Ratschbacher et al. 2000). The hornblende and biotite ages from JS349 are nearly equivalent, suggesting that the

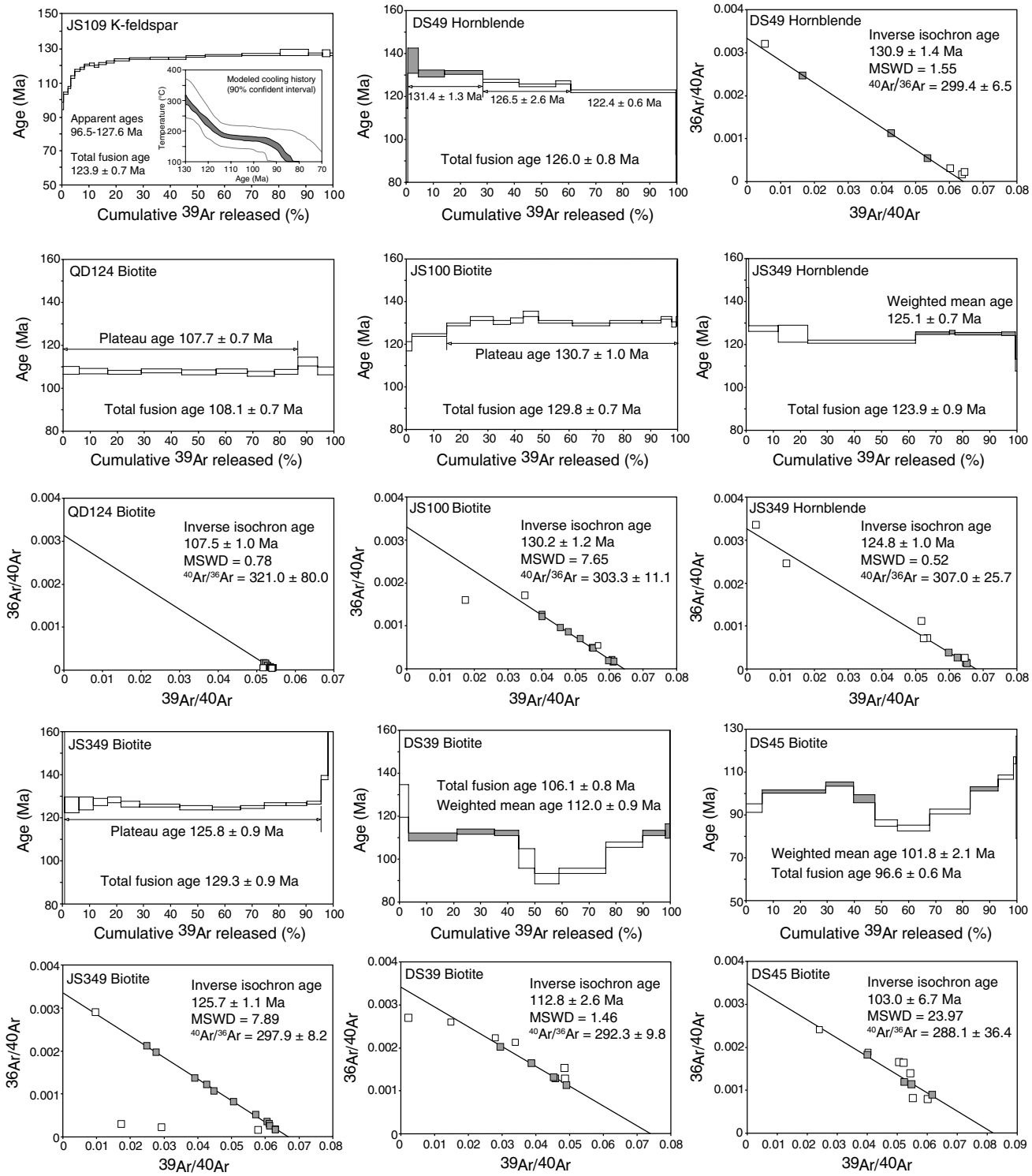

Fig. 10 $^{40}Ar/^{39}Ar$ age spectra and reverse isochron plots of the tectonites. The weighted mean ages were calculated using *solid steps*

XSF-N experienced a rapid cooling event at ca. 125 Ma. Moreover, the Lüyang pluton that cut the SWF and the XSF-N emplaced at 128.6 ± 0.8 Ma (Figs. 1, 9) (Yang et al. 2012). Thus, ductile shearing along the SWF and the XSF-N occurred prior to 128 Ma.

Unexpectedly, neither of the biotite samples (DS39 and DS45) from the XSF-S yielded an ideal plateau, but their apparent ages are mostly less than 120 Ma. Considering the XSF-S was mainly developed under greenschist facies conditions, we suggested that weighted mean ages of 112 and

102 Ma were approximate to the timing of ductile shearing along the XSF-S. In this regard, activity of the XSF-S is compatible with the late-stage ductile deformation of the SMF. Moreover, our K-feldspar MDD modeling result indicates that the XMF also recorded a late-stage cooling. The tectonic activation after 120 Ma may in part account for the mid-Cretaceous (110–90 Ma) reheating and subsequent cooling event documented in Ratschbacher et al. (2000).

Accordingly, we argued that the boundary faults warped around the CDD (including the XMF, SMF, SWF and XSF-N) experienced primary (early-stage) detachment during 142–130 Ma, while the XSF-S together with the SMF and perhaps part of the XMF was involved in secondary (late-stage) detachment at ca. 110 Ma.

Discussion

Multistage evolution of Dabieshan MCC

Although a thickened crust was inevitably produced by the Triassic NCB–SCB collision, seismic reflection data shows that the current Dabieshan has a normal crust with a thickness about 35 km (Wang et al. 2000a; Yuan et al. 2003). There is no magmatism related to the continental collision but voluminous Cretaceous granitoids. Systemic studies on geochronology and geochemistry of the Cretaceous granitoids indicate a crucial transition at ca.130 Ma, from adakitic to normal signatures (e.g., Wang et al. 2007; Xu et al. 2007, 2012a, b; Huang et al. 2008; Zhang et al. 2010; He et al. 2011, 2013). It appears that the migmatite–gneiss complex in the CDD also recorded two episodes of partial melting during the early Cretaceous. The early episode (145–130 Ma) corresponds to the extensive and intensive migmatization and associated metamorphism, while the late episode (129–120 Ma) are coeval with the large-scale magmatic activity (e.g., Wu et al. 2007; Xie et al. 2010; Wang et al. 2013; Chen et al. 2015). Above evidences indicate that the orogenic root of the Dabie orogen formed by the Triassic continental collision probably had been removed until the Early Cretaceous (Li et al. 2013d).

As stated before, the migmatite-corded dome in the central Dabieshan domain was defined as a cordilleran-type MCC with a complex detachment system (Fig. 11). A typical MCC usually displays two crustal layers separated by brittle–ductile transition. The consistently top-to-the-NW kinematics of the central Dabieshan complex and surrounding detachment faults indicates that the primary detachment was initiated from a flat-lying detachment zone at the middle crust level. Previous P–T estimate suggest that the migmatite in the CDD was formed at $P = 5$–7 kbar and $T = 700$–850 °C (Zhang et al. 1996, 2014; Wang et al. 2013). By using the Al-in-hornblende geobarometer, Ratschbacher et al. (2000) calculated an average exhumation depth of 18 km for the orthogneisses and granitic plutons in the CDD. It is thus speculated that the decoupling surface between the already exhumed HP–UHP slices of upper crust and the partially molten middle-lower crust probably behaved as the potential detachment zone.

Synthesizing previous and our new structural and geochronological data, we propose a tectonic scenario for the multistage evolution of the Dabieshan MCC (Fig. 12). (1) Crustal anatexis in the Dabieshan area commenced approximately at 145 Ma, which also represented onset of lithospheric extension. Accompanied with the migmatization in the central Dabieshan domain, a flat-lying detachment zone began to activate at the middle crustal level under a regional NW–SE extension. The ductile deformation before ca. 130 Ma was predominated by subhorizontal detachment with top-to-the-NW shearing under amphibolite facies conditions. Meanwhile, partial melting of the thickened lower crust produced the early-stage adakitic granitoids. (2) Delamination of the mantle lithosphere with part of the thickened lower crust at ca. 130 Ma reached the extensional climax. Subsequent upwelling of the asthenospheric mantle after ca. 130 Ma thereby induced the late-stage normal granitoids and mafic–ultramafic rocks. Buoyancy-driven ascent of the partially molten crust and magmas resulted in rapid exhumation of the MCC. During thermal doming, the mid-crustal detachment zone was warped to form the presently observed detachment faults around the CDD (including the XMF, SMF, SWF and XSF-N). These phenomena indicate that the Dabie orogen experienced isostatic rebound after the delamination. (3) After 120 Ma, magmatic activity in the Dabieshan area had nearly ceased. The detachment system probably experienced a migration accommodated to the crustal adjustment. This led to secondary detachment and final exhumation of the MCC under the ongoing NW–SE extension, when the ductile shearing was localized along the XSF-S, the SMF and perhaps part of the XMF. Later, brittle normal faulting reworked some of the pre-existing detachment faults such as the XMF and the SMF. The Tan-Lu fault was also activated as a normal fault during the Late Cretaceous to Cenozoic (Ratschbacher et al. 2000; Lin et al. 2009).

The Cretaceous anatexis in the Dabieshan area commenced at ca. 145 Ma, while removal of the orogenic root by delamination occurred at ca. 130 Ma. This raises a question where the heat source came from to be responsible for the partial melting during 145–130 Ma. Several possible mechanisms contributed to Cretaceous thermal evolution of the Dabie orogen: (1) radiogenic heat accumulation; (2) lithospheric stretching under an extensional regime; (3) abnormal mantle convection. These effects together can elevate the geothermal gradient of the orogenic wedge. When temperature of the middle-lower crust reached above

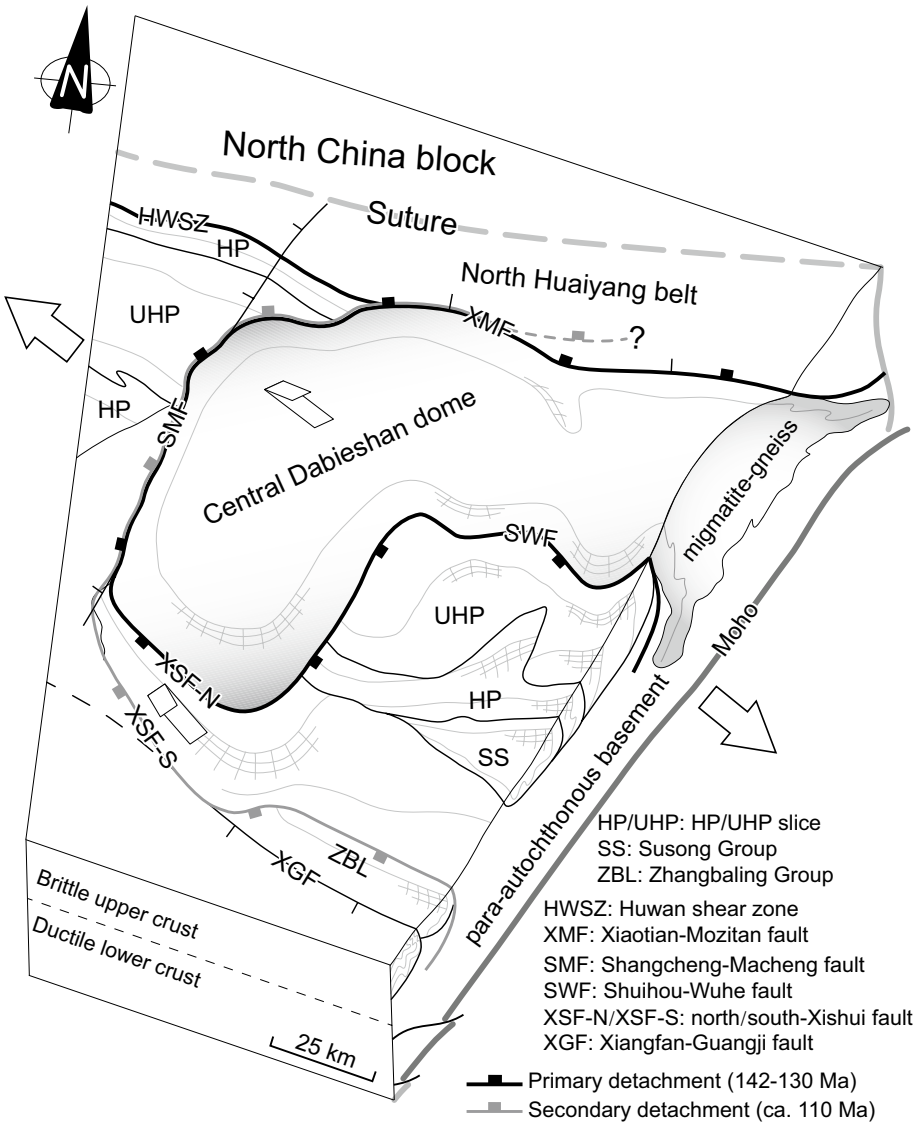

Fig. 11 Schematic block diagram shows the architecture of the Dabieshan MCC. *The arrows* indicate the top-to-the-NW motion of the detachment system under a NW–SW extension. The Moho offsets were inferred from geophysical surveys (Wang et al. 2000a; Yuan et al. 2003; Dong et al. 2004)

700 °C, partial melting commenced in the Dabieshan area. Presence of partially molten layer can significantly promote the potential of crustal flow, and increase gravitational instability of the orogenic root (Vanderhaeghe 2009). Consequently, this triggered delamination of the thickened lower crust in the Dabieshan.

Nature of the central Dabieshan complex

There is a long-standing debate on tectonic nature of the central Dabieshan complex over the past decades. Since the mafic–ultramafic rocks within the central Dabieshan complex usually show block-in-matrix structures, Xu et al. (1992) proposed that they are metamorphosed ophiolitic mélange, and thus represent the Triassic suture zone. In fact, such a structural feature was caused mostly by the Cretaceous migmatization. Except for a few blocks of metaperidotite and amphibolite, most of the mafic–ultramafic rocks are Cretaceous gabbro-pyroxenite intrusions (Jahn et al. 1999; Zhao et al. 2005; Huang et al. 2007; Dai et al. 2012). To account for the arc-like geochemical affinity of the orthogneisses in the CDD, Zhai et al. (1994, 1995) interpreted the central Dabieshan complex as a Paleozoic magmatic arc complex. After systematic investigations of representative metamorphic rocks from the CDD, Zhang et al. (1996) suggested that the central Dabieshan complex is a high-temperature amphibolite facies to granulite facies metamorphic terrane, which belongs to the Sino-Korean hanging wall above the subducted Yangtze plate. However, subsequent discovery of eclogite outcrops in the northern and southwestern parts of the CDD challenges the previous views. Eclogites within the CDD were firstly reported by Wei et al. (1998), and then by Xu et al. (2000) and Liu et al. (2000, 2005b, 2007a, 2011a, b). In particular, Tsai and Liou

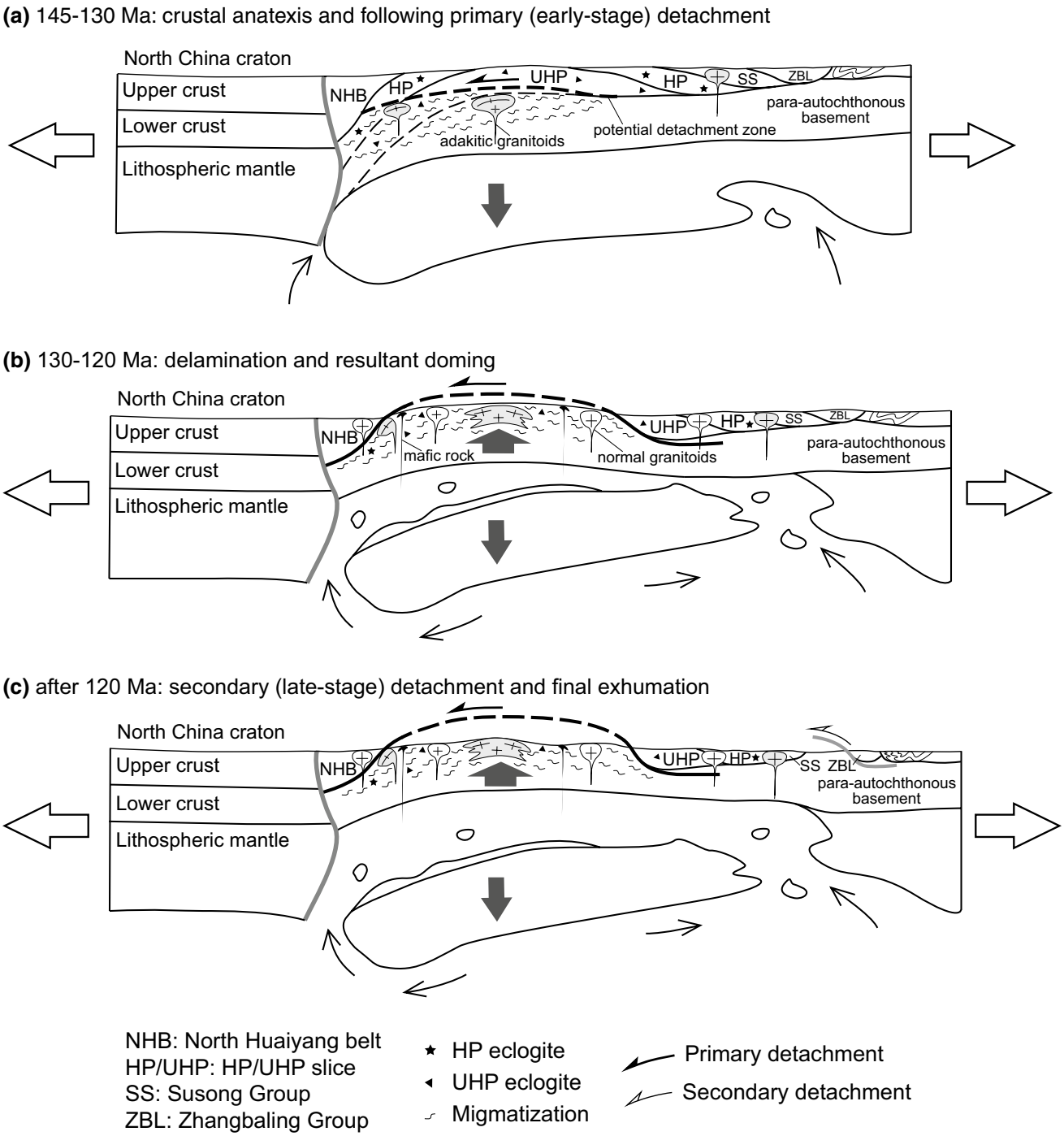

Fig. 12 Multistage evolution of the Dabieshan MCC (see text for details). It should be noted that the section is oblique to the stretching direction

(2000) and Malaspina et al. (2006) identified oriented exsolution lamellae in clinopyroxene or rod-like inclusions in garnet from eclogites (sensu lato) hosted by foliated metaperidotites in the CDD, suggesting there are relics of previous UHP metamorphism. Moreover, occurrence of diamond inclusion in the eclogite from the CDD is evident for UHP metamorphism (Xu et al. 2003). Besides, an HP eclogite xenolith had also been discovered within a Cretaceous granite to the west of Macheng (Lin et al. 2007).

On the other hand, a few Cretaceous zircon U–Pb ages for orthogneisses from the CDD had been reported, and Hacker et al. (1998) concluded that the entire central

Dabieshan complex is a Cretaceous magmatic complex and only a small portion of the complex existed prior to 137 Ma. Subsequently, numerous geochronological studies on the central Dabieshan complex show that inherited zircon cores with Neoproterozoic ages are widely occurred, and considerable zircons also yielded Triassic metamorphic ages (e.g., Liu et al. 2007b; Zhao et al. 2008; Xie et al. 2010). In view of UHP relicts and Triassic metamorphism in the CDD, the entire central Dabieshan complex was defined as a high-temperature UHP terrane that belongs to part of the deep-subducted Yangtze plate (Liu and Li 2008; Zheng 2008). On the contrary, it is noted that the residual UHP rocks outcrops sporadically and have tectonic contact with the underlying gneiss, Bryant et al. (2004) speculated the central Dabieshan complex is an extension of the Yangtze basement that was unaffected by the Triassic UHP metamorphism. The petrological evidences in support of UHP metamorphism for the central Dabieshan complex were also suspected by Zhang et al. (2009). Taking into account the spatial distribution of metamorphic ages (Triassic vs. Cretaceous), Zhao et al. (2008) alternatively assumed that the central Dabieshan complex is comprised of an upper UHP layer and a lower HP layer before the Cretaceous, which is separated by a décollement fault. They further suggested that the Cretaceous tectono-thermal event would result in preferred erosion of the upper UHP layer in the southern part rather than the southern part, and consequently Cretaceous ages occur in the southern part whereas Triassic ages are partly preserved in the northern part.

Above hypotheses are mainly based on petrological and geochronological evidences, and structural constraints is deficient. Origin of the CDD is undoubtedly the key to define the nature of the central Dabieshan complex. According to our structural analysis, the central Dabieshan complex was product of the Cretaceous crustal anatexis by consumption of pre-existing precursor rocks similar to the para-autochthonous basement and the HP–UHP slices in the SDTSS (Fig. 12). In other words, some pieces of but not all the central Dabieshan complex had experienced the Triassic UHP metamorphism. It is inadequate to conclude that all the Triassic ages from the central Dabieshan complex are related to UHP metamorphism. Moreover, the UHP rocks in the CDD and the SDTSS should belong to one coherent slice before the Cretaceous. This is in agreement with the fact that their peak UHP metamorphic ages are nearly synchronous within error (e.g., Li et al. 2000; Liu et al. 2011b). Nevertheless, petrological studies revealed that the UHP eclogites from the CDD had overprinted by granulite facies metamorphism, while the UHP rocks from the SDTSS only amphibolite facies retrogression (Liu et al. 2005b, 2007a, 2011a, b; Tong et al. 2011; Groppo et al. 2015). A reasonable interpretation is that the empennage of the UHP slice had already been exhumed to superficial crust after the Triassic exhumation, and was less affected by the Cretaceous anatexis. By contrast, the subducted forepart of the UHP slice still resided at a deep crustal level before the Cretaceous, as a result suffering granulite facies overprinting. During the Early Cretaceous, the MCC formation raised the CDD to a higher level, and most of the HP–UHP rocks previously in the central Dabieshan domain were extensively eroded. Meanwhile, the deep-sited HP–UHP rocks (including the granulitized UHP eclogites and host-gneisses) together with the para-autochthonous basement were involved in migmatization, giving birth to the central Dabieshan complex. It is especially interesting to note that the residual eclogites in the CDD yielded Cretaceous rutile U–Pb ages (Li et al. 2013c; Lin et al. 2015). This indicates that the UHP relicts in the CDD were exhumed from deep crustal level until the Cretaceous. Furthermore, the central Dabieshan complex was also partly overprinted granulite facies metamorphism associated with the Cretaceous migmatization (Hou et al. 2005; Tong et al. 2011). It is the complicated tectonic history that evoked a variety of viewpoints on nature of the central Dabieshan complex.

Cretaceous extension in the eastern Asian continent

The eastern margin of Eurasia experienced continent-scale lithospheric extension during the Late Mesozoic, and destruction of the North China Craton just occurred under such a tectonic setting. Cratonic destruction is manifested by large-scale lithospheric thinning, crustal detachment and magmatic activity (Menzies et al. 2007; Wu et al. 2008; Zhu et al. 2012b). Late Mesozoic extensional domes including MCCs were widely developed from Transbaikalia to North China (e.g., Zorin 1999; Davis et al. 2002; Liu et al. 2005a, 2013b; Lin and Wang 2006; Lin et al. 2008, 2011, 2013; Donskaya et al. 2008; Daoudene et al. 2009, 2013; Charles et al. 2011, 2012; Wang et al. 2011a, 2012b; Zhang et al. 2012; Zhu et al. 2015), as well as interior of South China (e.g., Faure et al. 1996; Lin et al. 2000; Zhu et al. 2010; Li et al. 2013b; Ji et al. 2014). Although distributed in different plates, most of the extensional domes share several common features: (1) their detachment faults are generally characterized by NW–SE trending lineation and top-to-the-NW or top-to-the-SE kinematics; (2) half-graben basins were always developed along the hanging walls of the detachments; (3) $^{40}Ar/^{39}Ar$ ages of syn-kinematic minerals concentrated at a narrow range mostly between 135 and 115 Ma, which indicates a uniform NW–SE extensional regime in the eastern Asian during the Early Cretaceous.

The term “post-collisional” has been favored by many authors to describe the Cretaceous magmatism in the Dabie orogen (e.g., Zhao et al. 2004, 2005, 2007, 2011; He et al.

2011, 2013; Li et al. 2013d), but there is at least 100 My interval between the Triassic NCB–SCB collision (ca. 250 Ma) and Cretaceous magmatic activity (143–117 Ma). Obviously, the Early Cretaceous tectono-thermal event has no direct relation with the Triassic orogeny. In view of the temporal-spatial framework of the extensional structures in the eastern Asian continent, the Dabieshan MCC with similar structural pattern and contemporaneous deformation age was reasonable to develop under the same tectonic setting as the destruction of the North China craton. The present architecture of the Dabieshan massif was mostly obtained by the Cretaceous extension. In fact, the whole Tongbai–Dabie–Sulu orogen was significantly reworked by the Cretaceous extension to different extent: the core of the Tongbai orogen formed a huge A-type extensional antiform; the central Dabieshan domain is occupied by a migmatite-cored MCC; the southern Sulu orogen is a "wedge-shaped" structure exhumed by a single detachment fault (Lin et al. 2015).

Thermal erosion (Xu 2001) and delamination (Gao et al. 2002) have been suggested as two main mechanisms for lithospheric thinning of the NCB, respectively, corresponding to chemical–mechanical (bottom-up) process and physical (top-down) process. Instability of thickened lithosphere is the premise of delamination. It is proposed that there was a plateau in eastern China during the Middle Jurassic to Early Cretaceous according to the temporal-spatial distribution of adakites (Zhang et al. 2001). However, recent research concerning on detrital source analysis of sediments revealed that the eastern NCB would be a subsidence rather than an elevation in the Jurassic (Li and Huang 2013; Li et al. 2013a). Thus, large-scale delamination is not supported in interior of stable craton, where the viable mechanism of lithospheric thinning was probably dominated by thermal erosion. It is worth noting that the Late Mesozoic extensional domes show some spatial regularity. MCCs are mostly superimposed upon the pre-existing orogenic belts around the NCB, such as the Mongol-Okhotsk belt (within the eastern part of the Central Asian orogenic belt), the Yinshan–Yanshan belt and the Tongbai–Dabie–Sulu belt. This indicates that delamination seems to be easily occurred along weak plate margins. In brief, thermal erosion and delamination are not mutually exclusive in cratonic destruction.

Geodynamic trigger of the Cretaceous continental-scale extension in the eastern Asian continent is still a mystery. Subduction of the Paleo-Pacific (including the Izanagi plate and Pacific plate) beneath the Eurasian continent is the most plausible model to account for the Cretaceous tectono-magmatism in eastern China, and destruction of the North China craton is no exception (e.g., Ren et al. 2002; Wu et al. 2005; Zhu et al. 2012a). However, the history of the Izanagi-Pacific subduction is less known (Engebretson et al. 1985; Maruyama et al. 1997; Sun et al. 2007). On the other hand, gravitational collapse of pre-existing orogenic plateau resulted from the collision between the Siberian craton and the Mongolia-NCB was suggested to be responsible for development of rift basins and exhumation of MCCs in the Mongol-Okhotsk belt and adjacent areas (Zorin 1999; Meng 2003). If all the Cretaceous extensional tectonics in the eastern Asia continent have the same geodynamic trigger, any single plate-margin effect alone fails to account for the fact that this extensional framework affected a vast region, from the Transbaikalia to SCB (for a detailed discussion, see Lin and Wang 2006; Lin et al. 2013). Alternatively, combination of the different tectonic regimes during the Late Mesozoic has been emphasized by some scholars, such as Pacific back-arc extension together with eastward tectonic escape resulted from collisions to the north (Siberia vs. Mongolia-NCB) and southwest (Lhasa vs. Qiangtang) (Ratschbacher et al. 2000); mantle upwelling induced by Mesozoic interactions between the NCB and surrounding plates (Zhai et al. 2007); post-orogenic collapse of the thickened crust derived from the Mongol-Okhotsk orogeny, and then superposed by a far-field effect of the Pacific subduction (Wang et al. 2011a, 2012b); after-effect of "eastern Asian multi-direction convergent tectonic system" associated with westward subduction of the Paleo-Pacific plate, northward subduction of the Neo-Tethys ocean and closure of the Mongol-Okhotsk ocean (Dong et al. 2008). Global-scale tectonic events such as break-up and dispersal of the Gondwanaland (Wilde et al. 2003) and Pacific superplume (Zhao et al. 2004, 2011; Zheng 2008) have also been put forward. Nevertheless, in the present state of knowledge, additional investigations such as numerical modeling are needed to reach a satisfying understanding on the geodynamic significance of the Late Mesozoic tectonics in the eastern Asian.

Conclusions

1. The architecture of the central Dabieshan domain exhibits as an orogen-scale MCC with multiple detachments. The central Dabieshan complex in the footwall and surrounding detachment faults recorded a consistently top-to-the-NW shearing. This indicates that the primary (early-stage) detachment was initiated from a flat-lying detachment zone at the middle crust level, probably corresponding to the decoupling surface between the already exhumed HP–UHP slices of upper crust and the underlying partially molten middle-lower crust. This mid-crustal detachment zone was warped as shear zones (including the XMF, SMF, SWF, and XSF-N) around the CDD during the doming. Moreover, the detachment system probably experienced a migration,

the XSF-S together with the SMF and perhaps part of the XMF was involved in secondary (late-stage) detachment.

2. Occurrence of the Dabieshan MCC experienced a multistage evolution: (1) 145–130 Ma: crustal anatexis and following primary detachment; (2) 130–120 Ma: delamination and resultant doming; (3) after 120 Ma: secondary detachment and final exhumation. Extensional collapse of the Dabie orogen manifested a combined effect of several geological processes at different lithospheric levels: removal of the orogenic root, ductile flow of the partially molten middle-lower crust and unroofing of the upper crust, which came into being the Dabieshan MCC.
3. The central Dabieshan complex is totally neither a Cretaceous magmatic complex or Triassic UHP terrane, nor just an extended part of the Yangtze basement. Instead, it was product of the Cretaceous crustal anatexis by consumption of pre-existing precursor rocks similar to the para-autochthonous basement and the HP–UHP slices in the SDTSS. Moreover, the UHP rocks in the CDD and the SDTSS could belong to one coherent slice before Cretaceous, but the former represent the deep-sited part that experienced a long period of residence at deep crustal level and consequently overprinted by granulite facies metamorphism.
4. We proposed that the Dabieshan MCC was developed under the same tectonic setting as the "destruction of the North China craton." The significant role of the Cretaceous reworking is beyond the previous knowledge, which destructed the Triassic architecture of the HP–UHP orogenic belt in east-central China. The case of the Dabieshan MCC constitutes a link of the Cretaceous extensional tectonics from Transbaikalia to SCB. It appears that the NW–SE extensional regime occurred throughout the eastern Asia continent during the Early Cretaceous; however, its geodynamic trigger is still a mystery.

Acknowledgments This work has been supported by the National Natural Science Foundation of China (Nos. 41225009, 41472193 and 41502202). Special thanks are due to Fei Wang and Lin Wu in IGGCAS for their help with the $^{40}Ar/^{39}Ar$ analyses. We are very grateful to Yunpeng Dong and Guang Zhu for their critical and constructive comments.

References

Ames L, Tilton GR, Zhou GZ (1993) Timing of collision of the Sino-Korean and Yangtze cratons: U–Pb zircon dating of coesite-bearing eclogites. Geology 21:339–342

Ames L, Zhou GZ, Xiong BC (1996) Geochronology and geochemistry of ultrahigh-pressure metamorphism with implications for collision of Sino-Korea and Yangtze cratons, central China. Tectonics 15:472–489

Ayers JC, Dunkle S, Gao S, Miller CF (2002) Constraints on timing of peak and retrograde metamorphism in Dabie Shan ultrahigh-pressure metamorphic belt, east central China, using U–Th–Pb dating of zircon and monazite. Chem Geol 186:315–331

Bryant DL, Ayers JC, Gao S, Miller CF, Zhang HF (2004) Geochemical, age, and isotopic constraints on the location of the Sino-Korean/Yangtze suture and evolution of the northern Dabie complex, east central China. Geol Soc Am Bull 116:698–717

Carswell DA, O'Brien PJ, Wilson RN, Zhai M (1997) Thermobarometry of phengite bearing eclogites in the Dabie Mountains of Central China. J Metamorph Geol 15:239–252

Charles N, Gumiaux C, Augier R, Chen Y, Lin W, Zhu RX (2011) Metamorphic core complex vs. synkinematic plutons in continental extension setting: insights from key structures (Shandong province, eastern China). J Asian Earth Sci 40:261–278

Charles N, Gumiaux C, Augier R, Chen Y, Faure M, Lin W, Zhu RX (2012) Metamorphic core complex dynamics and structural development: field evidences from the Liaodong peninsula (China, East Asia). Tectonophysics 560–561:22–50

Chavagnac V, Jahn BM (1996) Coesite-bearing eclogites from the Bixiling complex, Dabie Mountains, China: Sm–Nd ages, geochemical characteristics and tectonic implications. Chem Geol 133:29–51

Chavagnac V, Jahn BM, Villa IM, Whitehouse MJ, Liu DY (2001) Multichronometric evidence for an in situ origin of the ultrahigh-pressure metamorphic terrane of Dabieshan, China. J Geol 109:633–646

Chen TY, Niu BG, Liu ZG, Fu YL, Ren JS (1991) Geochronology of Yanshanian magmatism and metamorphism in the hinterland of the Dabie Mountains and their geologic implications. Acta Geol Sin 5:155–163

Chen JF, Xie Z, Liu SS, Li XM, Foland KA (1995) Cooling age of Dabie orogen, China, determined by $^{40}Ar/^{39}Ar$ and fission track techniques. Sci China Ser B 38:749–757

Chen NS, Sun M, You ZD, Malpas J (1998) Well-preserved garnet growth zoning in granulite from the Dabie Mountains, central China. J Metamorph Geol 16:213–222

Chen B, Jahn BM, Wei CJ (2002) Petrogenesis of Mesozoic granitoids in the Dabie UHP complex, central China: trace element and Nd–Sr isotope evidence. Lithos 60:67–88

Chen FK, Guo JH, Jiang LL, Siebel W, Cong BL, Satir M (2003) Provenance of the Beihuaiyang lower-grade metamorphic zone of the Dabie ultrahigh-pressure collisional orogen, China: evidence from zircon ages. J Asian Earth Sci 22:343–352

Chen Y, Ye K, Liu JB, Sun M (2006) Multistage metamorphism of the Huangtuling granulite, northern Dabie orogen, eastern China: implications for the tectonometamorphic evolution of subducted lower continental crust. J Metamorph Geol 24:633–654

Chen L, Ma CQ, She ZB, Mason R, Zhang JY, Zhang C (2009) Petrogenesis and tectonic implications of A-type granites in the Dabie orogenic belt, China: geochronological and geochemical constraints. Geol Mag 146:638–651

Chen RX, Ding BH, Zheng YF, Hu ZC (2015) Multiple episodes of anatexis in a collisional orogen: zircon evidence from migmatite in the Dabie orogen. Lithos 212–215:247–265

Cheng WQ, Yang KG, Kusky TM, Xiao H (2012) Kinematic and thermochronological constraints on the Xincheng–Huangpi fault and Mesozoic two-phase extrusion of the Tongbai–Dabie orogen belt. J Asian Earth Sci 60:160–173

Cui JJ, Liu XC, Dong SW, Hu JM (2012) U–Pb and $^{40}Ar/^{39}Ar$ geochronology of the Tongbai complex, central China: implications for Cretaceous exhumation and lateral extrusion of the Tongbai–Dabie HP/UHP terrane. J Asian Earth Sci 47:155–170

Dai LQ, Zhao ZF, Zheng YF, Zhang J (2012) The nature of orogenic lithospheric mantle: geochemical constraints from postcollisional mafic-ultramafic rocks in the Dabie orogen. Chem Geol 334:99–121

Daoudene Y, Gapais D, Ledru P, Cocherie A, Hocquet S, Donskaya TV (2009) The Ereendavaa Range (north-eastern Mongolia): an additional argument for Mesozoic extension throughout eastern Asia. Int J Earth Sci 98:1381–1393

Daoudene Y, Ruffet G, Cocherie A, Ledru P, Gapais D (2013) Timing of exhumation of the Ereendavaa metamorphic core complex (north-eastern Mongolia)—U–Pb and $^{40}Ar/^{39}Ar$ constraints. J Asian Earth Sci 62:98–116

Davis GA, Darby BJ (2010) Early cretaceous overprinting of the Mesozoic Daqing Shan fold-and-thrust belt by the Hohhot metamorphic core complex, Inner Mongolia, China. Earth Sci Front 17:1–20

Davis GA, Darby BJ, Zheng YD, Spell TL (2002) Geometric and temporal evolution of an extensional detachment fault, Hohhot metamorphic core complex, Inner Mongolia, China. Geology 30:1003–1006

Deng X, Yang KG, Polat A, Kusky TM, Wu KB (2014) Zircon U–Pb ages, major and trace elements, and Hf isotope characteristics of the Tiantangzhai granites in the North Dabie orogen, Central China: tectonic implications. Geol Mag 151:916–937

Dong YP, Santosh M (2016) Tectonic architecture and multiple orogeny of the Qinling orogenic belt, central China. Gondwana Res 29:1–40

Dong SW, Gao R, Cong BL, Zhao ZY, Liu XC, Li SZ, Li QS, Huang DD (2004) Crustal structure of southern Dabie ultrahigh-pressure orogen and Yangtze foreland from deep seismic reflection profile. Terra Nova 16:319–324

Dong SW, Zhang YQ, Chen XH, Long CX, Wang T, Yang ZY, Hu JM (2008) The formation and deformational characteristics of East Asia multi-direction convergent tectonic system in Late Jurassic. Acta Geosci Sin 29:306–317 **(in Chinese with English abstract)**

Dong YP, Zhang GW, Neubauer F, Liu XM, Genser J, Hauzenberger C (2011) Tectonic evolution of the Qinling orogen, China: review and synthesis. J Asian Earth Sci 41:213–237

Donskaya TV, Windley BF, Mazukabzov AM, Kröner A, Sklyarov EV, Gladkochub DP, Ponomarchuk VA, Badarch G, Reichow MK, Hegner E (2008) Age and evolution of late Mesozoic metamorphic core complexes in southern Siberia and northern Mongolia. J Geol Soc 165:405–421

Eide EA, McWilliams MO, Liou JG (1994) $^{40}Ar/^{39}Ar$ geochronology and exhumation of high-pressure to ultrahigh-pressure metamorphic rocks in east-central China. Geology 22:601–604

Engebretson DC, Cox A, Gordon RG (1985) Relative motion between oceanic and continental plates in the Pacific basin. Geol Soc Am Spec Paper 206:1–59

Faure M, Sun Y, Shu LS, Monié P, Charvet J (1996) Extensional tectonics within a subduction-type orogen. The case study of the Wugongshan dome (Jiangxi Province, SE China). Tectonophysics 263:77–108

Faure M, Lin W, Shu LS, Sun Y, Schärer U (1999) Tectonics of the Dabieshan (eastern China) and possible exhumation mechanism of ultrahigh-pressure rocks. Terra Nova 11:251–258

Faure M, Lin W, Schärer U, Shu LS, Sun Y, Arnaud N (2003) Continental subduction and exhumation of UHP rocks. Structural and geochronological insights from the Dabieshan (East China). Lithos 70:213–241

Gao S, Rudnick RL, Carlsonet RW, McDonough WF, Liu YS (2002) Re–Os evidence for replacement of ancient mantle lithosphere beneath the North China Craton. Earth Planet Sci Lett 198:307–322

Ge NJ, Xia QK, Wu YB, Hou ZH, Qin LP, Bo L (2003) Zircon U–Pb ages of Yanzihe gneiss from northern Dabie, China: evidence for Triassic metamorphism. Acta Petrol Sin 19:513–516 **(in Chinese with English abstract)**

Groppo C, Rolfo F, Liu YC, Deng LP, Wang AD (2015) P–T evolution of elusive UHP eclogites from the Luotian dome (North Dabie Zone, China): How far can the thermodynamic modeling lead us? Lithos 226:183–200

Hacker BR, Wang QC (1995) Ar/Ar geochronology of ultrahigh-pressure metamorphism in central China. Tectonics 14:994–1006

Hacker BR, Ratschbacher L, Webb L, Dong SW (1995) What brought them up? Exhumation of the Dabie Shan ultrahigh-pressure rocks. Geology 23:743–746

Hacker BR, Ratschbacher L, Webb L, Ireland T, Walker D, Dong S (1998) U/Pb zircon ages constrain the architecture of the ultrahigh-pressure Qinling–Dabie orogen, China. Earth Planet Sci Lett 161:215–230

Hacker BR, Ratschbacher L, Webb LE, McWilliams M, Ireland T, Dong S, Calvert A, Wenk HR (2000) Exhumation of ultrahigh-pressure continental crust in east-central China: late triassic-early jurassic tectonic unroofing. J Geophys Res 105:13339–13364

He YS, Li SG, Hoefs J, Huang F, Liu SA, Hou ZH (2011) Post-collisional granitoids from the Dabie orogen: new evidence for partial melting of a thickened continental crust. Geochim Cosmochim Acta 75:3815–3838

He YS, Li SG, Hoefs J, Kleinhanns IC (2013) Sr–Nd–Pb isotopic compositions of Early Cretaceous granitoids from the Dabie orogen: constraints on the recycled lower continental crust. Lithos 156–159:204–217

Hou ZH, Li SG, Chen NS, Li QL, Liu XM (2005) Sm–Nd and zircon SHRIMP U–Pb dating of Huilanshan mafic granulite in the Dabie Mountains and its zircon trace element geochemistry. Sci China Ser D 48:2081–2091

Hou QL, Liu Q, Li J, Zhang HY (2007) Late Mesozoic shear zones and its chronology in the Dabie Mountains, central China. Chin J Geol 42:114–123 **(in Chinese with English abstract)**

Huang F, Li SG, Dong F, Li QL, Chen FK, Wang Y, Yang W (2007) Recycling of deeply subducted continental crust in the Dabie Mountains, central China. Lithos 96:151–169

Huang F, Li SG, Dong F, He YS, Chen FK (2008) High-Mg adakitic rocks in the Dabie orogen, central China: implications for foundering mechanism of lower continental crust. Chem Geol 255:1–13

Jahn BM, Wu FY, Lo CH, Tsai CH (1999) Crust-mantle interaction induced by deep subduction of the continental crust: geochemical and Sr–Nd isotopic evidence from post-collisional mafic-ultramafic intrusions of the northern Dabie complex. Chem Geol 157:119–146

Ji WB, Lin W, Shi YH, Wang QC, Chu Y (2011) Structure and evolution of the Early Cretaceous Dabieshan metamorphic core complex. Chin J Geol 46:161–180 **(in Chinese with English abstract)**

Ji WB, Lin W, Faure M, Chu Y, Wu L, Wang F, Wang J, Wang QC (2014) Origin and tectonic significance of the Huangling massif within the Yangtze craton, South China. J Asian Earth Sci 86:59–75

Jian P, Kröner A, Zhou GZ (2012) SHRIMP zircon U–Pb ages and REE partition for high-grade metamorphic rocks in the North Dabie complex: insight into crustal evolution with respect to Triassic UHP metamorphism in east-central China. Chem Geol 328:49–69

Jiang LL, Liu YC, Wu WP, Li HM, Fang Z (2002) Zircon U–Pb age and its geological implications of the gray gneiss to the northern Manshuihe in the North Dabie Mountains. Geochimica 31:66–70 **(in Chinese with English abstract)**

Koppers AAP (2002) ArArCALC—software for $^{40}Ar/^{39}Ar$ age calculations. Comput Geosci 28:605–619

Li HY, Huang XL (2013) Constraints on the paleogeographic evolution of the North China Craton during the Late Triassic–Jurassic. J Asian Earth Sci 70–71:308–320

Li SG, Xiao YL, Liu DL, Chen YZ, Ge NJ, Zhang ZQ, Sun SS, Cong BL, Zhang RY, Hart SR (1993) Collision of the North China and Yangtse Blocks and formation of coesite-bearing eclogites: timing and processes. Chem Geol 109:89–111

Li SG, Jagoutz E, Chen YZ, Li QL (2000) Sm–Nd and Rb–Sr isotopic chronology and cooling history of ultrahigh pressure metamorphic rocks and their country rocks at Shuanghe in the Dabie Mountains, Central China. Geochim Cosmochim Acta 64:1077–1093

Li XP, Zheng YF, Wu YB, Chen FK, Gong B, Li YL (2004) Low-T eclogite in the Dabie terrane of China: petrological and isotopic constraints on fluid activity and radiometric dating. Contrib Mineral Petrol 148:443–470

Li SZ, Zhao GC, Zhang GW, Liu XC, Dong SW, Wang J, Liu X, Suo YH, Dai LM, Jin C, Liu LP, Hao Y, Liu ES, Wang J, Wang T (2010) Not all folds and thrusts in the Yangtze foreland belt are related to the Dabie orogen: insights from Mesozoic deformation south of the Yangtze River. Geol J 45:650–663

Li HY, Xu YG, Liu YM, Huang XL, He B (2013a) Detrital zircons reveal no Jurassic plateau in the eastern North China Craton. Gondwana Res 24:622–634

Li JH, Zhang YQ, Dong SW, Su JB, Li Y, Cui JJ, Shi W (2013b) The Hengshan low-angle normal fault zone: structural and geochronological constraints on the Late Mesozoic crustal extension in South China. Tectonophysics 606:97–115

Li QL, Yang YN, Shi YH, Lin W (2013c) Eclogite rutile U–Pb dating: constraint for formation and evolution of continental collisional orogen. China Sci Bull 58:2279–2284 **(in Chinese)**

Li SG, He YS, Wang SJ (2013d) Process and mechanism of mountain-root removal of the Dabie orogen—constraints from geochronology and geochemistry of post-collisional igneous rocks. Chin Sci Bull 58:4411–4417

Lin W, Wang QC (2006) Late Mesozoic extensional tectonics in North China block: a crustal response to the lithosphere removal of North China craton? Bull Soc Géol France 177:287–297

Lin W, Faure M, Monié P, Schärer U, Zhang LS, Sun Y (2000) Tectonics of SE China, new insights from the Lushan massif (Jiangxi Province). Tectonics 19:852–871

Lin W, Wang QC, Faure M, Sun Y, Shu LS, Scharer U (2003) Different deformation stages of the Dabieshan Mountains and UHP rocks exhumation mechanism. Acta Geol Sin 77:44–54 **(in Chinese with English abstract)**

Lin W, Wang QC, Faure M, Arnaud N (2005) Tectonic evolution of Dabie orogen: in the view from polyphase deformation of the Beihuaiyang metamorphic zone. Sci China Ser D 48:886–899

Lin W, Enami M, Faure M, Schärer U, Arnaud N (2007) Survival of eclogite xenolith in a Cretaceous granite intruding the central Dabieshan migmatite gneiss dome (eastern China) and its tectonic implications. Int J Earth Sci 96:707–724

Lin W, Faure M, Monié P, Schärer U, Panis D (2008) Mesozoic extensional tectonics in eastern Asia: the South Liaodong peninsula metamorphic core complex (NE China). J Geol 116:134–154

Lin W, Shi YH, Wang QC (2009) Exhumation tectonics of the HP-UHP orogenic belt in Eastern China: new structural–petrological insights from the Tongcheng massif, Eastern Dabieshan. Lithos 109:285–303

Lin W, Monié P, Faure M, Schärer U, Shi YH, Le Breton N, Wang QC (2011) Cooling paths of the NE China crust during the Mesozoic extensional tectonics: example from the south-Liaodong peninsula metamorphic core complex. J Asian Earth Sci 42:1048–1065

Lin W, Faure M, Chen Y, Ji WB, Wang F, Wu L, Charles N, Wang QC (2013) Late Mesozoic compressional to extensional tectonics in the Yiwulüshan massif, NE China and its bearing on the evolution of the Yinshan–Yanshan orogenic belt. Part I: structural analyses and geochronological constraints. Gondwana Res 23:54–77

Lin W, Ji WB, Faure M, Wu L, Li QL, Shi YH, Scharer U, Wang F, Wang QC (2015) Early Cretaceous extensional reworking of the Triassic HP–UHP metamorphic orogen in Eastern China. Tectonophysics 662:256–270

Liou JG, Zhang RY, Liu FL, Zhang ZM, Ernst WG (2012) Mineralogy, petrology, U–Pb geochronology, and geologic evolution of the Dabie–Sulu classic ultrahigh-pressure metamorphic terrane, East-Central China. Am Mineral 97:1533–1543

Liu YC, Li SG (2008) Detachment within subducted continental crust and multi-slice successive exhumation of ultrahigh-pressure metamorphic rocks: evidence from the Dabie–Sulu orogenic belt. Chin Sci Bull 53:3105–3119

Liu YC, Li SG, Xu ST, Li HM, Jiang LL, Chen GB, Wu WP, Su W (2000) U–Pb zircon ages of the eclogite and tonalitic gneiss from the northern Dabie Mountains, China and multi-overgrowths of metamorphic zircons. Geol J China Univ 6:417–423 **(in Chinese with English abstract)**

Liu JL, Davis GA, Lin ZY, Wu FY (2005a) The Liaonan metamorphic core complex, Southeastern Liaoning Province, North China: a likely contributor to Cretaceous rotation of Eastern Liaoning, Korea and contiguous areas. Tectonophysics 407:65–80

Liu YC, Li SG, Xu ST, Jahn BM, Zheng YF, Zhang ZQ, Jiang LL, Chen GB, Wu WP (2005b) Geochemistry and geochronology of eclogites from the northern Dabie Mountains, central China. J Asian Earth Sci 25:431–443

Liu DY, Jian P, Kröner A, Xu ST (2006) Dating of prograde metamorphic events deciphered from episodic zircon growth in rocks of the Dabie–Sulu UHP complex, China. Earth Planet Sci Lett 250:650–666

Liu YC, Li SG, Gu XF, Xu ST, Chen GB (2007a) Ultrahigh-pressure eclogite transformed from mafic granulite in the Dabie orogen, east-central China. J Metamorph Geol 25:975–989

Liu YC, Li SG, Xu ST (2007b) Zircon SHRIMP U–Pb dating for gneisses in northern Dabie high T/P metamorphic zone, central China: implications for decoupling within subducted continental crust. Lithos 96:170–185

Liu YC, Gu XF, Rolfo F, Chen ZY (2011a) Ultrahigh-pressure metamorphism and multistage exhumation of eclogite of the Luotian dome, North Dabie Complex Zone (central China): evidence from mineral inclusions and decompression textures. J Asian Earth Sci 42:607–617

Liu YC, Gu XF, Li SG, Hou ZH, Song B (2011b) Multistage metamorphic events in granulitized eclogites from the North Dabie complex zone, central China: evidence from zircon U–Pb age, trace element and mineral inclusion. Lithos 122:107–121

Liu JB, Zhang LM, Ye K, Su W, Cheng NF (2013a) Oxygen isotopes of whole-rock and zircon and zircon U–Pb ages of meta-rhyolite from the Luzhenguan Group and associated meta-granite in the northern Dabie Mountains. Acta Petrol Sin 29:1211–1524 **(in Chinese with English abstract)**

Liu JL, Shen L, Ji M, Guan HM, Zhang ZC, Zhao ZD (2013b) The Liaonan/Wanfu metamorphic core complexes in the Liaodong Peninsula: two stages of exhumation and constraints on the destruction of the North China Craton. Tectonics 32:1121–1141

Ma CQ, Li ZC, Ehlers C, Yang KG, Wang RJ (1998) A post-collisional magmatic plumbing system: mesozoic granitoid plutons from the Dabieshan high-pressure and ultrahigh-pressure metamorphic zone, east-central China. Lithos 45:431–456

Ma CQ, Yang KG, Ming HL, Lin GC (2004) The age of transformation for the Mesozoic crust of the Dabie orogen from compression to extension: evidences from granites. Sci China Ser D 47:453–462

Malaspina N, Hermann J, Scambelluri M, Compagnoniet R (2006) Multistage metasomatism in ultrahigh-pressure mafic rocks from the north Dabie complex (China). Lithos 90:19–42

Maruyama S, Isozaki Y, Kimura G, Terabayashi M (1997) Paleogeographic maps of the Japanese Islands: plate tectonic synthesis from 750 Ma to present. Island Arc 6:121–142

Mattauer M, Matte P, Malavieille J, Tapponnier P, Maluski H, Xu ZQ, Lu YL, Tang YQ (1985) Tectonics of Qinling belt: build-up and evolution of eastern Asia. Nature 317:496–500

Mattauer M, Matte P, Maluski H, Xu ZQ, Zhang QW, Wang YM (1991) La limite Chine du Nord-Chine du Sud au Paléozoïque et au Trias: nouvelles données structurales et radiométriques dans le massif du Dabieshan (chaîne des Qinling). Comptes Rendus de l'Académie des Sciences (Series II) 312:1227–1233

Meng QR (2003) What drove late Mesozoic extension of the northern China-Mongolia tract? Tectonophysics 369:155–174

Meng QR, Zhang GW (2000) Geologic framework and tectonic evolution of the Qinling orogen, central China. Tectonophysics 323:183–196

Menzies M, Xu YG, Zhang HF, Fan WM (2007) Integration of geology, geophysics and geochemistry: a key to understanding the North China Craton. Lithos 96:1–21

Okay AI (1993) Petrology of a diamond and coesite-bearing metamorphic terrain: Dabie Shan, China. Eur J Mineral 5:659–675

Okay AI, Xu ST, Sengör AMC (1989) Coesite from the Dabie Shan eclogites, central China. Eur J Mineral 1:595–598

Okay AI, Sengör AMC, Satir M (1993) Tectonics of an ultrahigh-pressure metamorphic terrane: the Dabie Shan/Tongbai Shan orogen, China. Tectonics 12:1320–1334

Ratschbacher L, Hacker BR, Webb LE, McWilliams M, Ireland T, Dong S, Clavert A, Chateigner D, Wenk HR (2000) Exhumation of the ultrahigh-pressure continental crust in east central China: cretaceous and Cenozoic unroofing and the Tan-Lu fault. J Geophys Res 105:13303–13338

Ratschbacher L, Hacker BR, Calvert A, Webb LE, Grimmer JC, McWilliams MO, Ireland T, Dong S, Hu J (2003) Tectonics of the Qinling (central China): tectonostratigraphy, geochronology, and deformation history. Tectonophysics 366:1–53

Ratschbacher L, Franz L, Enkelmann E, Jonckheere R, Pörschke A, Hacker BR, Dong S, Zhang Y (2006) The Sino-Korean-Yangtze suture, the Huwan detachment, and the Paleozoic-Tertiary exhumation of (ultra)high-pressure rocks along the Tongbai–Xinxian–Dabie Mountains. In: Hacker BR, McClelland WC, Liou JG (eds) Ultrahigh-pressure metamorphism: deep continental subduction. Geological Society of America Special Paper 403, pp 45–75

Ren JY, Tamaki K, Li ST, Zhang JX (2002) Late Mesozoic and Cenozoic rifting and its dynamic setting in Eastern China and adjacent areas. Tectonophysics 344:175–205

Rowley DB, Xue F, Tucker RD, Peng ZX, Baker J, Davis A (1997) Ages of ultrahigh pressure metamorphism and protolith orthogneisses from eastern Dabie Shan: U/Pb zircon geochronology. Earth Planet Sci Letters 151:191–203

Shi YH, Wang QC (2006) Changes in the peak P–T conditions across the upper contact of the UHP terrane, Dabie Shan, China: gradational or abrupt? J Metamorph Geol 24:803–822

Shi YH, Wang CS, Kang T, Xu XF, Lin W (2012) Petrological characteristics and zircon U–Pb age for Susong metamorphic complex rocks in Anhui Province. Acta Petrol Sin 28:3389–3402 **(in Chinese with English abstract)**

Shi YH, Lin W, Ji WB, Wang QC (2014) The architecture of the HP–UHP Dabie massif: new insights from geothermobarometry of eclogites, and implication for the continental exhumation processes. J Asian Earth Sci 86:38–58

Sun WD, Ding X, Hu YH, Li XH (2007) The golden transformation of the Cretaceous plate subduction in the west Pacific. Earth Planet Sci Lett 262:533–542

Suo ST, Zhong ZQ, You ZD (2000) Extensional deformation of post ultrahigh-pressure metamorphism and exhumation process of ultrahigh-pressure metamorphic rocks in the Dabie massif, China. Sci China Ser D 43:225–236

Suo ST, Zhong ZQ, Zhou HW, You ZD, Zhang HF, Zhang L (2005) Tectonic evolution of the Dabie–Sulu UHP and HP metamorphic belts, east-central China: structural record in UHP rocks. Int Geol Rev 47:1207–1221

Tong LX, Jahn BM, Zheng YF (2011) Diverse P–T paths of the northern Dabie complex in central China and its reworking in the early Cretaceous. J Asian Earth Sci 42:633–640

Tsai CH, Liou JG (2000) Eclogite-facies relics and inferred ultrahigh-pressure metamorphism in the North Dabie Complex, central-eastern China. Am Mineral 85:1–8

Vanderhaeghe O (2009) Migmatites, granites and orogeny: flow modes of partially-molten rocks and magmas associated with melt/solid segregation in orogenic belts. Tectonophysics 477:119–134

Wang GC, Yang WR (1996) Structural and chronological evidence of the Luotian dome in the core of the eastern Dabie Mountains, central China. J China Univ Geosci 21:524–528

Wang XM, Liou JG, Mao HK (1989) Coesite-bearing eclogite from the Dabie Mountains in central China. Geology 17:1085–1088

Wang XM, Liou JG, Maruyama S (1992) Coesite-bearing eclogites from the Dabie Mountains, central China: petrogenesis, P-T paths, and implications for regional tectonics. J Geol 100:231–250

Wang QC, Liu XH, Maruyama S, Cong BL (1995) Top boundary of the Dabie UHPM rocks, central China. J Southeast Asian Earth Sci 11:295–300

Wang XD, Neubauer F, Genser J, Yang WR (1998) The Dabie UHP unit, central China: a Cretaceous extensional allochthon superposed on a Triassic orogen. Terra Nova 10:260–267

Wang CY, Zeng RS, Mooney WD, Hacker BR (2000a) A crustal model of the ultrahigh-pressure Dabie Shan orogenic belt, China, derived from deep seismic refraction profiling. J Geophys Res 105:10857–10869

Wang YT, Li JL, Liu DL, Wu YG, Fu YT, Wu J (2000b) ^{40}Ar–^{39}Ar dating of the Shangcheng-Macheng fault belt in the Dabie orogen and its significance. Geol Rev 46:611–615 **(in Chinese with English abstract)**

Wang JH, Sun M, Deng SX (2002) Geochronological constraints on the timing of migmatization in the Dabie Shan, East-central China. Eur J Mineral 14:513–524

Wang E, Meng QR, Burchfiel BC, Zhang GW (2003) Mesozoic large-scale lateral extrusion, rotation, and uplift of the Tongbai–Dabie Shan belt in east China. Geology 31:307–310

Wang Q, Wyman DA, Xu JF, Jian P, Zhao ZH, Li CF, Xu W, Ma JL, He B (2007) Early Cretaceous adakitic granites in the northern Dabie complex, central China: implications for partial melting and delamination of thickened lower crust. Geochim Cosmochim Acta 71:2609–2636

Wang GC, Wang P, Liu C, Wang A, Ye RQ (2008) Geochronology constraints on transformation age from ductile to brittle deformation of the Shangma fault and its tectonic significance, Dabieshan, central China. J China Univ Geosci 19:97–109

Wang T, Zheng YD, Zhang JJ, Zeng LS, Donskaya T, Guo L, Li JB (2011a) Pattern and kinematic polarity of late Mesozoic extension in continental NE Asia: perspectives from metamorphic core complexes. Tectonics 30:TC6007. doi:10.1029/2011TC002896

Wang YS, Xiang BW, Zhu G, Jiang DZ (2011b) Structural and geochronological evidence for Early Cretaceous orogen-parallel extension of the ductile lithosphere in the northern Dabie orogenic belt, East China. J Struct Geol 33:362–380

Wang SJ, Li SG, An SC, Hou ZH (2012a) A granulite record of multistage metamorphism and REE behavior in the Dabie orogen: constraints from zircon and rock-forming minerals. Lithos 136–139:109–125

Wang T, Guo L, Zheng YD, Donskaya TV, Gladkochub D, Zeng LS, Li JB, Wang Y, Mazukabzov A (2012b) Timing and processes of late Mesozoic mid-lower-crustal extension in continental NE Asia and implications for the tectonic setting of the destruction of the North China Craton: mainly constrained by zircon U–Pb ages from metamorphic core complexes. Lithos 154:315–345

Wang SJ, Li SG, Chen LJ, He YS, An SC, Shen J (2013) Geochronology and geochemistry of leucosomes in the North Dabie Terrane, East China: implication for post-UHPM crustal melting during exhumation. Contrib Mineral Petrol 165:1009–1029

Wang F, Wang QC, Lin W, Wu L, Shi WB, Feng HL, Zhu RX (2014) $^{40}Ar/^{39}Ar$ geochronology of the North China and Yangtze Cratons: new constraints on Mesozoic cooling and cratonic destruction under East Asia. J Geophys Res 119:3700–3721

Wawrzenitz N, Romer RL, Oberhänsli R, Dong S (2006) Dating of subduction and differential exhumation of UHP rocks from the Central Dabie Complex (E-China): constraints from microfabrics, Rb–Sr and U–Pb isotope systems. Lithos 89:174–201

Webb LE, Hacker BR, Ratschbacher L, McWilliams MO, Dong S (1999) Thermochronologic constraints on deformation and cooling history of high- and ultrahigh-pressure rocks in the Qinling–Dabie orogen, eastern China. Tectonics 18:621–638

Wei CJ, Shan ZG, Zhang LF, Wang SG, Chang ZG (1998) Determination and geological significance of the eclogites from the northern Dabie Mountains, central China. Chin Sci Bull 43:253–256

Wilde SA, Zhou XH, Nemchin AA, Sun M (2003) Mesozoic crust-mantle interaction beneath the North China craton: a consequence of the dispersal of Gondwanaland and accretion of Asia. Geology 31:817–820

Wu YB, Zheng YF (2013) Tectonic evolution of a composite collision orogen: an overview on the Qinling–Tongbai–Hong'an–Dabie–Sulu orogenic belt in central China. Gondwana Res 23:1402–1428

Wu FY, Lin JQ, Wilde SA, Zhang XO, Yang JH (2005) Nature and significance of the Early Cretaceous giant igneous event in eastern China. Earth Planet Sci Lett 233:103–119

Wu YB, Zheng YF, Zhao ZF, Gong B, Liu XM, Wu FY (2006) U–Pb, Hf and O isotope evidence for two episodes of fluid-assisted zircon growth in marble-hosted eclogites from the Dabie orogen. Geochim Cosmochim Acta 70:3743–3761

Wu YB, Zheng YF, Zhang SB, Zhao ZF, Wu FY, Liu XM (2007) Zircon U–Pb ages and Hf isotope compositions of migmatite from the north Dabie terrane in China: constraints on partial melting Journal of Metamorphic. Geology 25:991–1009

Wu YB, Zheng YF, Gao S, Jiao WF, Liu YS (2008) Zircon U–Pb age and trace element evidence for Paleoproterozoic granulite-facies metamorphism and Archean crustal rocks in the Dabie orogen. Lithos 101:308–322

Xie Z, Chen JF, Zhang YF, Zhang X, Li HM, Zhou TX (2001a) Zircon U–Pb dating of the metamorphic rocks of different grades from the southern part of the Dabie terrain in China. Phys Chem Earth A 26:685–693

Xie Z, Chen JF, Zhang X, Gao TS, Dai SQ, Zhou TX, Li HM (2001b) Zircon U–Pb dating of gneiss from Shizhuhe in north Dabie and its geologic implications. Acta Petrol Sin 17:139–144 **(in Chinese with English abstract)**

Xie Z, Zheng YF, Zhao ZF, Wu YB, Wang ZR, Chen JF, Liu XM, Wu FY (2006) Mineral isotope evidence for the contemporaneous process of Mesozoic granite emplacement and gneiss metamorphism in the Dabie orogen. Chem Geol 231:214–235

Xie Z, Chen JF, Cui YR (2010) Episodic growth of zircon in UHP orthogneisses from the north Dabie terrane of east-central China: implications for crustal architecture of a collisional orogen. J Metamorph Geol 28:979–995

Xu YG (2001) Thermo-tectonic destruction of the Archean lithospheric keel beneath the Sino-Korean craton in China: evidence, timing and mechanism. Phys Chem Earth A 26:747–757

Xu JW, Zhu G, Tong WX, Cui KR, Liu Q (1987) Formation and evolution of the Tancheng-Lujiang wrench fault system: a major shear system to the northwest Pacific ocean. Tectonophysics 134:273–310

Xu ST, Okay AI, Ji SY, Sengör AMC, Su W, Liu YC, Jiang LL (1992) Diamond from the Dabie Shan metamorphic rocks and its implication for tectonic setting. Science 256:80–82

Xu ST, Su W, Liu YC, Wang RC, Jiang LL, Wu WP (2000) Discovery of the eclogite and its petrography in the northern Dabie Mountain. Chin Sci Bull 45:273–278

Xu CH, Zhou ZY, Ma CQ, Reiners PW (2002a) Geochronological constraints on 140–85 Ma thermal doming extension in the Dabie orogen, central China. Sci China Ser D 45:802–816

Xu ST, Liu YC, Jiang LL, Wu WP, Chen GB (2002b) Architecture and kinematics of the Dabie Mountains. University of Science and Technology of China Press, Hefei, pp 1–133 **(in Chinese with English abstract)**

Xu ST, Liu YC, Chen GB, Compagnoni R, Rolfo F, He MC, Liu HF (2003) New finding of microdiamonds in eclogites from Dabie–Sulu region in central-eastern China. Chin Sci Bull 48:988–994

Xu HJ, Ma CQ, Ye K (2007) Early cretaceous granitoids and their implications for the collapse of the Dabie orogen, eastern China: SHRIMP zircon U–Pb dating and geochemistry. Chem Geol 240:238–259

Xu HJ, Ma CQ, Zhang JF, Ye K (2012a) Early Cretaceous low-Mg adakitic granites from the Dabie orogen, eastern China: petrogenesis and implications for destruction of the over-thickened lower continental crust. Gondwana Res 23:190–207

Xu HJ, Ma CQ, Zhang JF (2012b) Generation of Early Cretaceous high-Mg adakitic host and enclaves by magma mixing, Dabie orogen, Eastern China. Lithos 142–143:182–200

Xu ST, Wu WP, Lu YQ, Wang DH (2012c) Tectonic setting of the low-grade metamorphic rocks of the Dabie Orogen, central eastern China. J Struct Geol 37:134–149

Xue F, Rowley DB, Tucker RD, Peng ZX (1997) U–Pb zircon ages of granitiod rocks in the north Dabie complex, eastern Dabie Shan, China. J Geol 105:744–753

Xue HM, Dong SW, Liu XC (2003) Geochemical characteristics and U–Pb zircon dating of Dashankeng monzonitic granitic gneiss in northeastern Dabie Mountains. Adv Earth Sci 18:192–199 **(in Chinese with English abstract)**

Yang KG, Cheng WQ, Zhu QB, Li XG (2012) A discussion on two times southward thrusting of Xiangfan–Guangji fault in South Dabie orogen, central China. Geol Rev 57:480–494 **(in Chinese with English abstract)**

Yuan XC, Klemperer SL, Teng WB, Liu LX, Chetwin E (2003) Crustal structure and exhumation of the Dabie Shan ultrahigh-pressure orogen, eastern China, from seismic reflection profiling. Geology 31:435–438

Zhai MG, Cong BL, Zhang Q, Wang QC (1994) The northern Dabieshan terrain: a possible Andean-type arc. Int Geol Rev 36:867–883

Zhai MG, Cong BL, Zhao ZY, Wang QC, Wang G, Jiang LL (1995) Petrological-tectonic units in the coesite-bearing metamorphic terrain of the Dabie Mountains, central China and their geotectonic implications. J Southeast Asian Earth Sci 11:1–13

Zhai MG, Fan QC, Zhang HF, Sui JL, Shao JA (2007) Lower crustal processes leading to Mesozoic lithospheric thinning beneath eastern North China: underplating, replacement and delamination. Lithos 96:36–54

Zhang RY, Liou JG, Tsai CH (1996) Petrogenesis of a high-temperature metamorphic terrane: a new tectonic interpretation for the north Dabieshan, central China. J Metamorph Geol 14:319–333

Zhang Q, Qian Q, Wang EQ, Wang Y, Zhao TP, Hao J, Guo GJ (2001) An east China plateau in Mid-Late Yanshannian period: implication from adakites. Chin J Geol 36:248–255 **(in Chinese with English abstract)**

Zhang RY, Liou JG, Ernst WG (2009) The Dabie–Sulu continental collision zone: a comprehensive review. Gondwana Res 16:1–26

Zhang C, Ma CQ, Holtz F (2010) Origin of high-Mg adakitic magmatic enclaves from the Meichuan pluton, southern Dabie orogen (central China): implications for delamination of the lower continental crust and melt-mantle interaction. Lithos 119:467–484

Zhang BL, Zhu G, Jiang DZ, Li CC, Chen Y (2012) Evolution of the Yiwulushan metamorphic core complex from distributed to localized deformation and its tectonic implications. Tectonics 31:TC4018. doi:10.1029/2012TC003104

Zhang C, Holtz F, Koepke J, Berndt J, Ma CQ (2014) Decompressional anatexis in the migmatite core complex of northern Dabie orogen, eastern China: petrological evidence and Ti-in-quartz thermobarometry. Lithos 202–203:227–236

Zhao ZF, Zheng YF, Wei CS, Wu YB (2004) Zircon isotope evidence for recycling of subducted continental crust in post-collisional granitoids from the Dabie terrane in China. Geophys Res Lett 31:L22602. doi:10.1029/2004GL021061

Zhao ZF, Zheng YF, Wei CS, Wu YB, Chen FK, Jahn BM (2005) Zircon U–Pb age, element and C–O isotope geochemistry of post-collisional mafic-ultramafic rocks from the Dabie orogen in east-central China. Lithos 83:1–28

Zhao ZF, Zheng YF, Wei CS, Wu YB (2007) Post-collisional granitoids from the Dabie orogen in China: zircon U–Pb age, element and O isotope evidence for recycling of subducted continental crust. Lithos 93:248–272

Zhao ZF, Zheng YF, Wei CS, Chen FK, Liu XM, Wu FY (2008) Zircon U–Pb ages, Hf and O isotopes constrain the crustal architecture of the ultrahigh-pressure Dabie orogen in China. Chem Geol 253:222–242

Zhao ZF, Zheng YF, Wei CS, Wu FY (2011) Origin of postcollisional magmatic rocks in the Dabie orogen: implications for crust-mantle interaction and crustal architecture. Lithos 126:99–114

Zhao T, Zhu G, Lin SZ, Wang HT (2016) Indentation-induced tearing of a subducting continent: evidence from the Tan-Lu Fault Zone, East China. Earth Sci Rev 152:14–36

Zheng YF (2008) A perspective view on ultrahigh-pressure metamorphism and continental collision in the Dabie–Sulu orogenic belt. Chin Sci Bull 53:3081–3104

Zheng YF, Wu YB, Chen FK, Gong B, Li L, Zhao ZF (2004) Zircon U–Pb and oxygen isotope evidence for a large-scale ^{18}O depletion event in igneous rocks during the Neoproterozoic. Geochim Cosmochim Acta 68:4145–4165

Zheng YF, Zhou JB, Wu YB, Xie Z (2005) Low-grade metamorphic rocks in the Dabie–Sulu orogenic belt: a passive-margin accretionary wedge deformed during continent subduction. Int Geol Rev 47:851–871

ZhengYF W, Gong B, Chen RX, Tang J, Zhao ZF (2007) Tectonic driving of Neoproterozoic glaciations: evidence from extreme oxygen isotope signature of meteoric water in granite. Earth Planet Sci Lett 256:196–210

Zhong ZQ, Suo ST, You ZD (1999) Regional scale extensional tectonic pattern of ultrahigh-pressure and high-pressure metamorphic belts from the Dabie massif, China. Int Geol Rev 41:1033–1041

Zhu G, Wang YS, Liu GS, Niu ML, Xie CL, Li CC (2005) $^{40}Ar/^{39}Ar$ dating of strike-slip motion on the Tan-Lu fault zone, East China. J Struct Geol 27:1379–1398

Zhu G, Xie CL, Chen W, Xiang BW, Hu ZQ (2010) Evolution of the Hongzhen metamorphic core complex: evidence for Early Cretaceous extension in the eastern Yangtze craton, eastern China. Geol Soc Am Bull 122:506–516

Zhu G, Jiang DZ, Zhang BL, Chen Y (2012a) Destruction of the eastern North China Craton in a backarc setting: evidence from crustal deformation kinematics. Gondwana Res 22:86–103

Zhu RX, Xu YG, Zhu G, Zhang HF, Xia QK, Zheng TY (2012b) Destruction of the north China Craton. Sci China Earth Sci 55:1565–1587

Zhu G, Chen Y, Jiang DZ, Lin SZ (2015) Rapid change from compression to extension in the North China Craton during the Early Cretaceous: evidence from the Yunmengshan metamorphic core complex. Tectonophysics 656:91–110

Zorin YA (1999) Geodynamics of the western part of the Mongolia–Okhotsk collisional belt, Trans-Baikal region (Russia) and Mongolia. Tectonophysics 306:33–56